

# Analytical Solutions of 3D Maxwell's Equations via Infinite-Order Curl-Operator Expansions

David Wei Ge<sup>a,\*</sup>

<sup>a</sup>*Retired, formerly with Microsoft, Redmond, USA*

---

## Abstract

Solving Maxwell's equations in open-space settings with general initial conditions and source terms remains a fundamental challenge. We address this problem through an operator-based construction, developing an infinite-order curl-operator expansion that yields analytical solutions as function-to-function mappings from initial data and source terms to electromagnetic fields. The framework is applied to representative cases, including Gaussian initial conditions, Gaussian sources, harmonic sources, and Ricker wavelet sources. In these applications, a family of deformed sine and cosine functions emerges naturally, enabling explicit analytical representations of the solutions. The analysis further shows that these deformed trigonometric functions are intrinsically embedded in the general solution formulas, with their structure determined by the initial conditions and source terms. The results are compared with numerical simulations based on the Yee FDTD method and further support a systematic study of mesh refinement effects. This study reveals a consistent trend: FDTD results become largely insensitive to further step size reduction once the step size is sufficiently small. The results also demonstrate that the analytical solutions provide theoretical insight into electromagnetic field behavior and serve as practical benchmarks for computational electromagnetics.

*Keywords:* Maxwell's equations, Analytical solutions, Partial differential equations (PDEs), Finite-difference time-domain (FDTD), Wave propagation

---

## 1. Introduction

<sup>1</sup> Electromagnetic phenomena in three dimensions are governed by Maxwell's equations. Although computational techniques, such as the finite-difference time-domain (FDTD) method, are the dominant tools for simulating 3D problems [1–9],

---

\*Corresponding author

*Email address:* [gexiaobao.usa@gmail.com](mailto:gexiaobao.usa@gmail.com) (David Wei Ge)

<sup>1</sup>submitted manuscript

they exhibit intrinsic errors arising from truncation of higher-order derivatives and discretization, including numerical dispersion, grid anisotropy, and spurious non-physical artifacts such as apparent superluminal signal propagation [8, 10]. Despite substantial progress in both numerical and analytical approaches, constructing analytical time-domain solutions for general 3D initial and source configurations remains challenging; most existing methods rely on potential formulations with gauge freedom or on integral representations that are often analytically intractable [11–14]. In this work, we address this challenge through a systematic operator-based construction, developing an infinite-order curl-operator expansion that eliminates truncation error and yields compact analytical solutions, thereby providing a general solution mapping framework for time-domain Maxwell problems.

Central to this approach is the distinction between a mapping—the correspondence between input and output functions—and a transformation, the explicit formula that realizes this correspondence. Classical Taylor series define self-mappings on analytic functions. The theorems presented here extend this concept by establishing mappings from analytic inputs to distinct outputs, enabling exact function-to-function transformations that define a general solution mapping for Maxwell’s equations in the time domain. The one-dimensional formulation of this approach is reported in [15]; the present work extends these results to three dimensions.

From this perspective, the resulting formulations offer several advantages over conventional numerical schemes: (1) each point in space–time can be evaluated independently, without requiring a computational domain or artificial boundaries; (2) the underlying physical properties of the equations are preserved, avoiding numerical artifacts such as dispersion and grid anisotropy; and (3) the analytical structure provides insights into field behavior that are often difficult to extract from numerical data alone. These analytical solutions are intended to complement, rather than replace, numerical methods such as the FDTD method and finite element time-domain method, serving as rigorous reference fields for verification and analysis.

The remainder of this paper is organized as follows. Section 2 introduces the problem formulation and defines the corresponding solutions. Section 3 presents the solution formulas, based on a Time-Space theorem proved in Appendix A. Section 4 presents a series of case studies, with the necessary symbols and auxiliary formulas provided in Appendix B.

## 2. The Problem

The following notation is used throughout the paper. Capital letters denote three-dimensional vector functions, and lowercase letters denote scalars. A lowercase variable with an over-arrow denotes a three-dimensional vector variable. The symbol  $0$  represents either a scalar or a vector, depending on the context.

### 2.1. Definition of the problem

Consider the following three-dimensional Maxwell's equations in open space:

$$\frac{\partial H(x, y, z, \theta)}{\partial \theta} = -\frac{1}{\eta} \nabla \times E(x, y, z, \theta) \quad (1)$$

$$\frac{\partial E(x, y, z, \theta)}{\partial \theta} = \eta \nabla \times H(x, y, z, \theta) - \eta J(x, y, z, \theta) \quad (2)$$

$$H(x, y, z, 0) = F_h(x, y, z) \quad (3)$$

$$E(x, y, z, 0) = F_e(x, y, z) \quad (4)$$

where  $\eta = \sqrt{\mu/\epsilon}$ ,  $\theta = ct$ ,  $c = 1/\sqrt{\epsilon\mu}$ , and

$$x, y, z, t \in \mathbb{R}; \epsilon, \mu \in \mathbb{R}_{>0}; F_h, F_e \in C^\infty(\mathbb{R}^3, \mathbb{R}^3); J, H, E \in C^\infty(\mathbb{R}^4, \mathbb{R}^3)$$

where  $\epsilon$  and  $\mu$  are constants,  $x, y, z$  are space coordinates,  $t$  is time, function  $J(x, y, z, \theta)$  is the source term, functions  $F_h(x, y, z)$  and  $F_e(x, y, z)$  are the initial values. The equations are with dimensionless units [2, 9]. For convenience,  $\theta$  is referred to as time. The initial values satisfy the following conditions.

$$\nabla \cdot F_h(x, y, z) = 0 \quad (5)$$

$$\nabla \cdot F_e(x, y, z) = 0 \quad (6)$$

### 2.2. Definition of the solution

A function pair  $\{ H(x, y, z, \theta), E(x, y, z, \theta) \}$  is a solution to the problem if and only if it satisfies (1), (2), (3), and (4).

### 2.3. Solution as a function mapping

Taking functions  $J(x, y, z, \theta)$ ,  $F_h(x, y, z)$  and  $F_e(x, y, z)$  as the input, function pair  $\{ H(x, y, z, \theta), E(x, y, z, \theta) \}$  as the output, the definitions of the problem and its solution define a function-to-function mapping:

$$\{ J(x, y, z, \theta), F_h(x, y, z), F_e(x, y, z) \} \rightarrow \{ H(x, y, z, \theta), E(x, y, z, \theta) \} \quad (7)$$

For practical analysis, we divide the general problem into two fundamental sub-cases.

**Initial-value problem:**

$$\{ J(x, y, z, \theta) \equiv 0, F_h(x, y, z), F_e(x, y, z) \} \rightarrow \{ H(x, y, z, \theta), E(x, y, z, \theta) \} \quad (8)$$

**Source-driven problem:**

$$\{ J(x, y, z, \theta), F_h(x, y, z) \equiv 0, F_e(x, y, z) \equiv 0 \} \rightarrow \{ H(x, y, z, \theta), E(x, y, z, \theta) \} \quad (9)$$

### 3. The solutions

#### Definition of higher orders of curls:

For a 3D vector  $F$  its higher order curls are defined by

$$\nabla^0 \times F = F$$

$$\nabla^n \times F = \underbrace{\nabla \times \nabla \times \dots \times \nabla \times F}_n, n \geq 0$$

**Theorem 1. *The uniqueness of the solutions.*** *If a function-pair  $H, E \in C^\infty(\mathbb{R}^4, \mathbb{R}^3)$  is a solution of Maxwell's equations (1 - 4) then the solution is unique.*

*Proof.* Suppose there are two solutions  $\{H_1, E_1\}$  and  $\{H_2, E_2\}$  in  $C^\infty(\mathbb{R}^4, \mathbb{R}^3)$  for the same initial values and the source term. Denote

$$D_h = H_1 - H_2$$

$$D_e = E_1 - E_2$$

Because both  $\{H_1, E_1\}$  and  $\{H_2, E_2\}$  satisfy (1 - 4) we have the following source-free null-initial value Maxwell's equations for  $D_h$  and  $D_e$ :

$$\frac{\partial D_h}{\partial \theta} = -\frac{1}{\eta} \nabla \times D_e \quad (10)$$

$$\frac{\partial D_e}{\partial \theta} = \eta \nabla \times D_h \quad (11)$$

$$D_h(x, y, z, 0) = 0 \quad (12)$$

$$D_e(x, y, z, 0) = 0 \quad (13)$$

Because  $D_h, D_e \in C^\infty(\mathbb{R}^4, \mathbb{R}^3)$ , (12) and (13) give

$$\nabla^n \times D_h(x, y, z, 0) = 0, \forall n \geq 0 \quad (14)$$

$$\nabla^n \times D_e(x, y, z, 0) = 0, \forall n \geq 0 \quad (15)$$

Substitute (10), (11) (14) and (15) into (A.1 - A.4) with  $J$  and all its derivatives removed, we have

$$\frac{\partial^n D_h(x, y, z, 0)}{\partial \theta^n} = 0, \forall n \geq 0$$

$$\frac{\partial^n D_e(x, y, z, 0)}{\partial \theta^n} = 0, \forall n \geq 0$$

By Taylor series, the above two equations give

$$D_h(x, y, z, \theta) = 0$$

$$D_e(x, y, z, \theta) = 0$$

Thus, we have

$$H_1(x, y, z, \theta) = H_2(x, y, z, \theta)$$

$$E_1(x, y, z, \theta) = E_2(x, y, z, \theta)$$

$\therefore$  The solution is unique.  $\square$

**Theorem 2. Initial value solution.** *The function-to-function transformation defined by formulas (16) and (17) provides a mapping that satisfies the initial-value problem described by (8) provided that the corresponding series exist and converge.*

$$\begin{aligned} H(x, y, z, \theta) &= F_h(x, y, z) \\ &+ \sum_{n=0}^{\infty} (-1)^{n+1} \frac{\theta^{2(n+1)}}{(2(n+1))!} \nabla^{2(n+1)} \times F_h(x, y, z) \\ &+ \frac{1}{\eta} \sum_{n=0}^{\infty} (-1)^{n+1} \frac{\theta^{2n+1}}{(2n+1)!} \nabla^{2n+1} \times F_e(x, y, z) \end{aligned} \quad (16)$$

$$\begin{aligned} E(x, y, z, \theta) &= F_e(x, y, z) \\ &+ \sum_{n=0}^{\infty} (-1)^{n+1} \frac{\theta^{2(n+1)}}{(2(n+1))!} \nabla^{2(n+1)} \times F_e(x, y, z) \\ &+ \eta \sum_{n=0}^{\infty} (-1)^n \frac{\theta^{2n+1}}{(2n+1)!} \nabla^{2n+1} \times F_h(x, y, z) \end{aligned} \quad (17)$$

*Proof.* Present  $H(x, y, z, \theta)$  and  $E(x, y, z, \theta)$  in Taylor series and regroup the series into

$$\begin{aligned} H(x, y, z, \theta) &= \sum_{n=0}^{\infty} \frac{\partial^{2n} H(x, y, z, 0)}{\partial \theta^{2n}} \frac{\theta^{2n}}{(2n)!} + \sum_{n=0}^{\infty} \frac{\partial^{2n+1} H(x, y, z, 0)}{\partial \theta^{2n+1}} \frac{\theta^{2n+1}}{(2n+1)!} \\ E(x, y, z, \theta) &= \sum_{n=0}^{\infty} \frac{\partial^{2n} E(x, y, z, 0)}{\partial \theta^{2n}} \frac{\theta^{2n}}{(2n)!} + \sum_{n=0}^{\infty} \frac{\partial^{2n+1} E(x, y, z, 0)}{\partial \theta^{2n+1}} \frac{\theta^{2n+1}}{(2n+1)!} \end{aligned}$$

Substituting the temporal derivatives with the curls given by (A.1 - A.4), we reach (16) and (17).  $\square$

**Theorem 3. Source driven solution.** *The function-to-function transformation defined by formulas (18) and (19) provides a mapping that satisfies the source-driven problem described by (9) provided that the corresponding series exist and converge.*

$$\begin{aligned}
H(x, y, z, \theta) &= \sum_{n=0}^{\infty} \frac{\theta^{2(n+1)}}{(2(n+1))!} \sum_{k=0}^n (-1)^k \nabla^{2k+1} \times \frac{\partial^{2(n-k)} J(x, y, z, 0)}{\partial \theta^{2(n-k)}} \\
&+ \sum_{n=1}^{\infty} \frac{\theta^{2n+1}}{(2n+1)!} \sum_{k=1}^n (-1)^{k+1} \nabla^{2k-1} \times \frac{\partial^{2(n-k)+1} J(x, y, z, 0)}{\partial \theta^{2(n-k)+1}}
\end{aligned} \tag{18}$$

$$\begin{aligned}
E(x, y, z, \theta) &= \eta \sum_{n=0}^{\infty} \frac{\theta^{2(n+1)}}{(2(n+1))!} \sum_{k=0}^n (-1)^{k+1} \nabla^{2k} \times \frac{\partial^{2(n-k)+1} J(x, y, z, 0)}{\partial \theta^{2(n-k)+1}} \\
&+ \eta \sum_{n=0}^{\infty} \frac{\theta^{2n+1}}{(2n+1)!} \sum_{k=0}^n (-1)^{k+1} \nabla^{2k} \times \frac{\partial^{2(n-k)} J(x, y, z, 0)}{\partial \theta^{2(n-k)}}
\end{aligned} \tag{19}$$

The proof of this theorem follows that of the formulas for the initial-value solution and is omitted for brevity.

The solution formulas for the source-driven problem directly yield the following theorem.

**Theorem 4.** *If  $\{H(x, y, z, \theta), E(x, y, z, \theta)\}$  is the solution of the source driven problem for the source term  $J(x, y, z, \theta)$  then  $\{kH(x, y, z, \theta), kE(x, y, z, \theta)\}$  is the solution for the source driven problem for the source term  $kJ(x, y, z, \theta), \forall k \in \mathbb{R}$ .*

#### 4. Case studies

In these case studies, calculations of analytical solutions are made using high-precision arithmetic with 5000 decimal digits. The summation series are truncated to 600 terms. This choice ensures robust convergence of the numerical results and serves as a reference implementation rather than an optimized computational strategy. The resulting numeric data for electromagnetic fields are presented in 3D drawings.

In the figures, colored three-dimensional grids indicate coordinate planes: (x,y), (y,z), and (z,x) are shown in red, blue, and yellow, respectively. Vectors are depicted as straight line segments in three dimensions, with lengths proportional to their magnitudes. A consistent length scale is maintained within each figure group.

Electromagnetic field snapshots are presented within an 8-meter cube:

$$H(i\Delta_s, j\Delta_s, k\Delta_s, q\Delta_\theta)$$

$$\begin{aligned}
& E(i\Delta_s, j\Delta_s, k\Delta_s, q\Delta_\theta) \\
& i, j, k = 0, \pm 1, \pm 2, \dots, \pm 10 \\
& q = 0, 1, 2, \dots, 50
\end{aligned}$$

In [15], comparisons with FDTD were added in response to reviewers' suggestions and were performed for only one case study. In the present work, FDTD comparisons are included for all case studies. The computational domains are chosen sufficiently large so that the data within the central 8-meter cube remain unaffected by boundary effects, while data in the outer regions are discarded.

The effects of reducing the FDTD spatial step size  $\Delta_s$  are investigated. The initial spatial and temporal step sizes are  $\Delta_s = 0.4$  and  $\Delta_\theta = 0.23$ , respectively. The simulations are repeated using the reduced spatial step sizes defined by (20), while the temporal step sizes are adjusted to preserve the Courant number.

$$\begin{aligned}
\Delta_s &= 0.4; n = 0 \\
\Delta_{sn} &= \Delta_s / (2n); n = 1, 2, \dots
\end{aligned} \tag{20}$$

Because of the staggered-grid structure of the Yee-FDTD algorithm, vector components are not defined at identical spatial locations. Accurate comparisons therefore require separate analytical evaluations at the staggered locations of all six field components, leading to substantial computational cost. In this paper, only  $E_x$  is evaluated at the 11 spatial points defined by (21). These points are chosen arbitrarily and are not intended to represent any special property of the Yee-FDTD algorithm.

$$\begin{aligned}
& E_x(s\Delta_s + \Delta_s/2, 5\Delta_s, 5\Delta_s, q\Delta_\theta) \\
& s = 0, 1, 2, \dots, 10 \\
& q = 0, 1, 2, \dots, 50
\end{aligned} \tag{21}$$

There are multiple possible approaches for evaluating the differences between the FDTD and analytical solutions. In this paper, two statistics are considered: (1) the maximum difference, defined by (22); and (2) the cumulative difference, defined by (23).

$$err_{max}(n) = \max_q \frac{\max_s |E_{xa} - E_{xn}|}{\max_s |E_{xa}|} \tag{22}$$

$$err_{sum}(n) = \sum_q \frac{\sum_s |E_{xa} - E_{xn}|}{\max_s |E_{xa}|} \tag{23}$$

where  $E_{xa}$  is the  $E_x$  component calculated from the analytical solution, and  $E_{xn}$  is the  $E_x$  component obtained from the Yee-FDTD simulation using the spatial

step size defined by (20). Comparisons of  $E_{xa}$  and  $E_{xn}$  are evaluated at the same spatial and temporal locations defined by (21).

Because  $err_{max}(n)$  and  $err_{sum}(n)$  are computed from only a limited number of data points, they are intended as indicators rather than rigorous accuracy measures. If the difference in  $err_{max}(n)$  between two simulations is sufficiently large, the simulation with the smaller value may be considered more accurate. However, when the difference is small, no definitive conclusion regarding relative accuracy can be made. Moreover, no universal threshold exists for determining whether a difference is sufficiently large or small.

Reducing the spatial step size is computationally expensive. In our studies, the FDTD simulation with  $\Delta_s = 0.4$  required 0.06 seconds to complete 50 temporal steps using a 24-core CPU. When the spatial step size was reduced to  $\Delta_s/22$ , the computation time increased to 24 hours, while the required memory increased from 19 MB to 164 GB. The large number of computations also accumulates floating-point roundoff errors. Double-precision arithmetic was used in the FDTD simulations. Numerical errors may be reduced by using higher-precision arithmetic, although this would significantly increase both computation time and memory usage. In contrast, the analytical calculations were performed using 5000-digit precision.

Another major factor affecting simulation accuracy is the truncation of higher-order derivatives. The Yee-FDTD method uses first-order derivative approximations and neglects higher-order terms, whereas the analytical calculations in this work include derivatives up to 1201st order. In addition, FDTD approximates derivatives using field values at neighboring grid points instead of exact derivatives at individual spatial points. The analytical calculations, by contrast, use exact pointwise derivatives.

The variables used in the case studies are defined in Appendix B.1. The deformed sine and cosine functions forming the closed-form analytical solutions are defined in Appendix B.2. By ‘‘closed-form,’’ we mean that the formulas defining the functions  $H(x, y, z, \theta)$  and  $E(x, y, z, \theta)$  contain neither differential nor integral operators.

#### 4.1. Case-study 1: Gaussian initial-value

The following initial values are used.

$$F_h(x, y, z) = 0 \tag{24}$$

$$F_e(x, y, z) = \exp(-ar^2)\vec{b} \tag{25}$$

By applying (B.53) and (B.54) to (25) and substituting the results into (16) and (17), we obtain the following closed-form analytical solution:

$$\begin{aligned}
H(x, y, z, \theta) &= \\
& - \frac{1}{\eta\sqrt{a}} \exp(-ar^2) \text{sinp}(\xi, \sigma)_{3,0,0} \vec{d} \\
& + \frac{1}{\eta\sqrt{a}} \exp(-ar^2) \left( \frac{1}{2} \text{sinp}(\xi, \sigma)_{1,0,1} + 2 \text{sinp}(\xi, \sigma)_{2,0,0} \right) \vec{c} \\
E(x, y, z, \theta) &= \exp(-ar^2) \text{cosp}(\xi, \sigma)_{2,0,0} \vec{b}
\end{aligned}$$

where  $\xi = \sqrt{a}\theta$ ,  $\sigma = 2\sqrt{ar}$ .

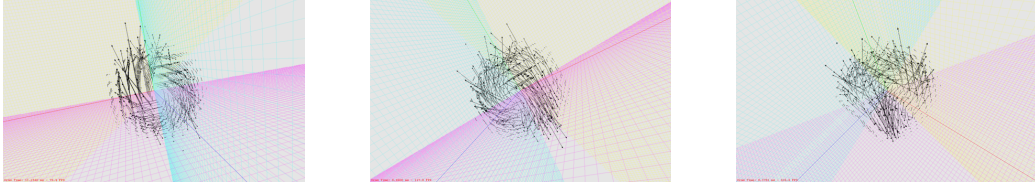


Figure 1: Gaussian initial value viewed from different perspectives.

Fig.1 shows the initial value viewed from different 3D perspectives.

From the analytical solution, the following characteristics of the electromagnetic fields can be observed:

- The direction of the electric field is  $\vec{b}$ , which remains constant over time.
- The magnetic field is confined to a two-dimensional plane spanned by the vectors  $\vec{c}$  and  $\vec{s}$ , as  $\vec{d} = g(x^2 - z^2)\vec{s}$ .
- Since  $\vec{c} \cdot \vec{b} = 0$  and  $\vec{s} \cdot \vec{b} = 0$ , it follows that  $H \cdot E = 0$ . Thus, the electric and magnetic fields are everywhere orthogonal.
- For energy transfer, using

$$\begin{aligned}
\vec{b} \times \vec{c} &= (x^2 + y^2)\vec{s} - (x^2 - z^2)\vec{c} \\
\vec{b} \times \vec{s} &= (x^2 - z^2)\vec{s} - r^2\vec{c}
\end{aligned}$$

it follows that the Poynting vector is also confined to the plane spanned by  $\vec{c}$  and  $\vec{s}$ .

- Since an analytical expression for the Poynting vector is available, the characteristics of energy transfer can be examined analytically in a systematic manner.

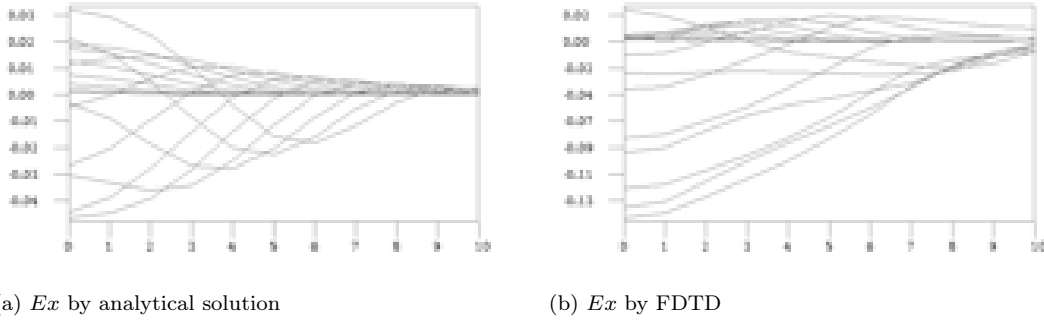


Figure 2:  $E_x$  by the analytical solution and by FDTD simulation (case study 1).

Figure 2 compares  $E_x$  computed from the analytical solution with that obtained from FDTD simulations. Figure 2a presents snapshots of  $E_x(x + \Delta_s/2, y, z, \theta)$  evaluated using the analytical formulas, while Figure 2b shows the corresponding results from the FDTD simulation. The two sets of results highlight agreement in the global field structure, while also exhibiting systematic differences attributable to discretization effects inherent to the FDTD scheme.

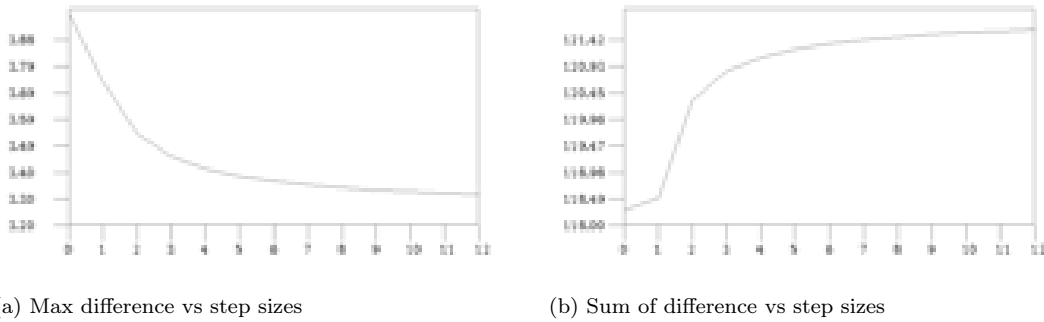


Figure 3: Effects of step sizes on FDTD simulations (Case-study 1).

Figure 3a shows the maximum difference between  $E_x$  values computed from the analytical solution and those obtained from FDTD simulations, while Figure 3b shows the cumulative absolute difference. The variable  $n$  on the horizontal axis denotes the spatial step size defined in (20). These figures lead to the following observations:

- The maximum difference decreases as the step size is reduced.
- The cumulative difference increases as the step size is reduced.
- Further reduction of the step size yields diminishing changes once the step size is sufficiently small.

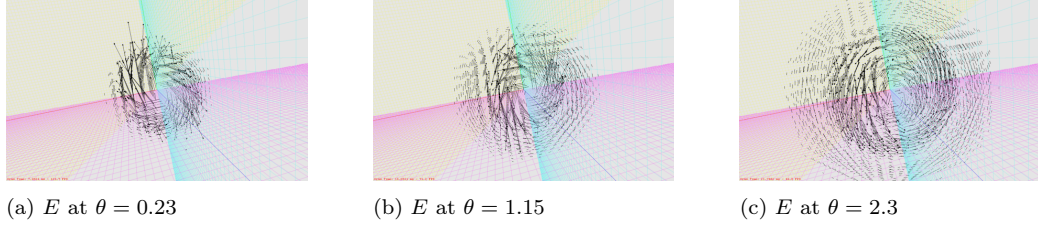


Figure 4: Electric field by analytical solution.  $q = 1, 5, 10$  (Case-study 1).

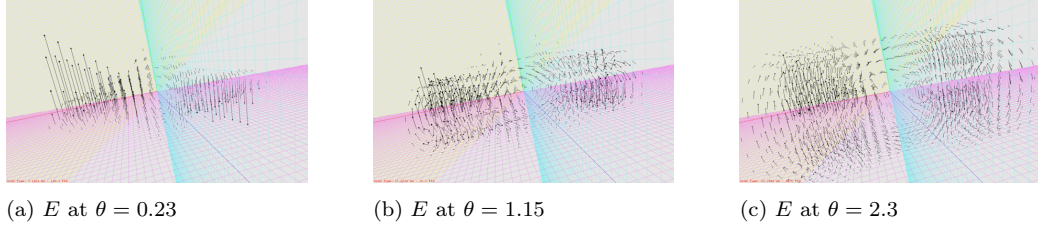


Figure 5: Electric field by FDTD.  $q = 1, 5, 10$  (Case-study 1).

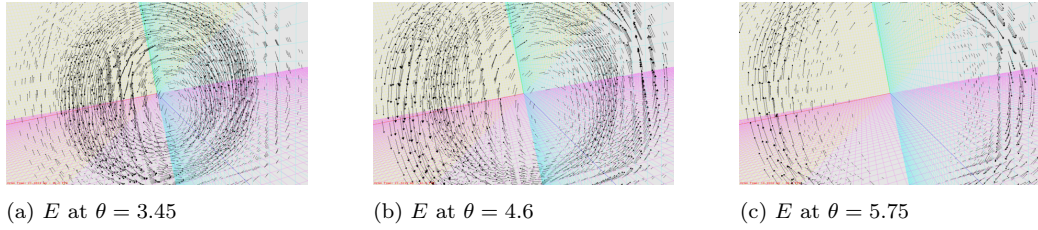


Figure 6: Electric field by analytical solution.  $q = 15, 20, 25$  (Case-study 1).

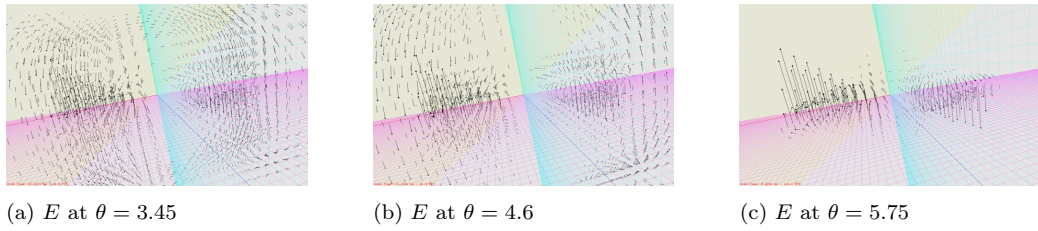


Figure 7: Electric field by FDTD.  $q = 15, 20, 25$  (Case-study 1).

Figures 4 and 6 show six snapshots of the electric field obtained from the analytical solution, while Figures 8 and 10 present the corresponding magnetic field snapshots. Figures 5, 7, 9, and 11 show the FDTD simulation results, with vector components visualized at coincident spatial locations for comparison.

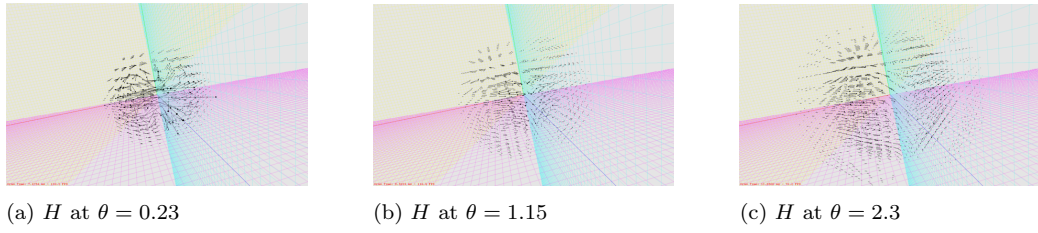


Figure 8: Magnetic field by analytical solution.  $q = 1, 5, 10$  (Case-study 1).

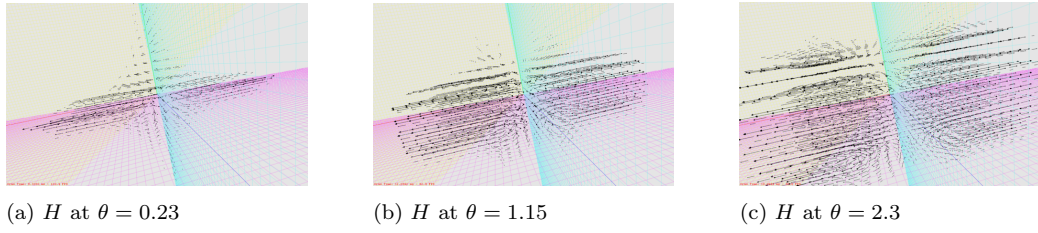


Figure 9: Magnetic field by FDTD.  $q = 1, 5, 10$  (Case-study 1).

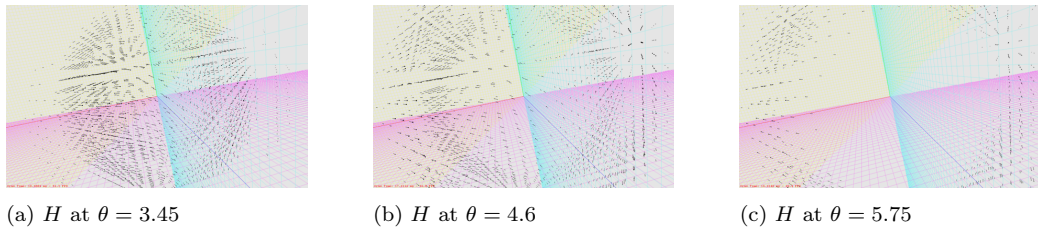


Figure 10: Magnetic field by analytical solution.  $q = 15, 20, 25$  (Case-study 1).

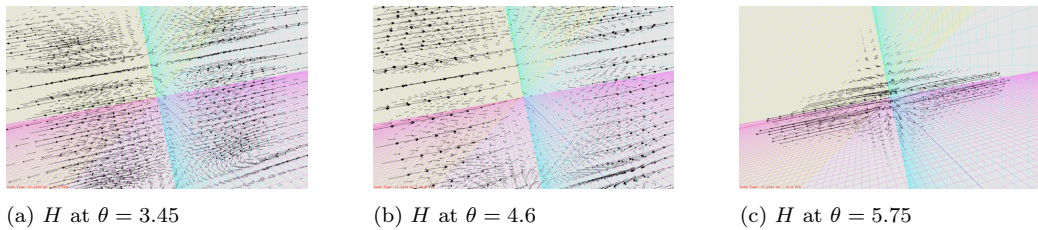


Figure 11: Magnetic field by FDTD.  $q = 15, 20, 25$  (Case-study 1).

These three-dimensional visualizations reveal significant discrepancies between the analytical and FDTD results for this case. This behavior contrasts with the other case studies, where close agreement is observed. Notably, the present case is formulated as an initial-value problem, whereas the others are source-driven; the extent to which this distinction contributes to the observed discrepancies remains to be investigated.

#### 4.2. Case-study 2: Gaussian source

The following source is used.

$$J(x, y, z, \theta) = \exp(-ar^2)\vec{z} \quad (26)$$

(26) gives

$$\frac{\partial^n J(x, y, z, \theta)}{\partial \theta^n} = 0; \forall n > 0 \quad (27)$$

By applying (B.55) and (B.56) to (26) and substituting the results and (27) into (18) and (19), we obtain the following closed-form analytical solution:

$$H(x, y, z, \theta) = -\frac{1}{a} \exp(-ar^2) \text{cosp}(\xi, \sigma)_{1,1,0} \vec{h} \quad (28)$$

$$E(x, y, z, \theta) = \frac{2\eta}{\sqrt{a}} \exp(-ar^2) \text{sinp}(\xi, \sigma)_{2,1,0} \vec{e} - \frac{\eta}{\sqrt{a}} \exp(-ar^2) (\xi - 4\text{sinp}(\xi, \sigma)_{1,1,0} + \sigma^2 \text{sinp}(\xi, \sigma)_{2,1,0}) \vec{z} \quad (29)$$

where  $\xi = \sqrt{a}\theta$ ,  $\sigma = 2\sqrt{ar}$ .

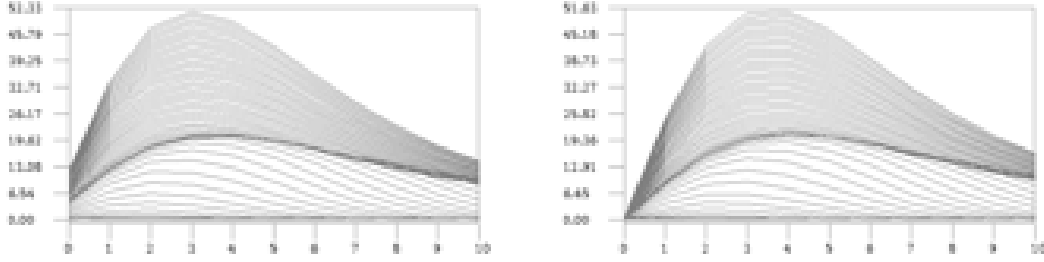
From the analytical solution, the following characteristics of the electromagnetic fields can be observed:

- The direction of the magnetic field is  $\vec{f}$ , as  $\vec{h} = g\vec{f}$ , which remains constant over time.
- The electric field is confined to a two-dimensional plane spanned by the vectors  $\vec{z}$  and  $\vec{s}$ , as  $\vec{e} = gz\vec{s}$ .
- Since  $\vec{z} \cdot \vec{f} = 0$  and  $\vec{s} \cdot \vec{f} = 0$ , it follows that  $H \cdot E = 0$ . Thus, the electric and magnetic fields are everywhere orthogonal.
- For energy transfer, using

$$\begin{aligned} \vec{f} \times \vec{z} &= -\vec{s} + z\vec{z} \\ \vec{f} \times \vec{s} &= -z\vec{s} + r^2\vec{z} \end{aligned}$$

it follows that the Poynting vector is also confined to the plane spanned by  $\vec{s}$  and  $\vec{z}$ .

- Since an analytical expression for the Poynting vector is available, the characteristics of energy transfer can be examined analytically in a systematic manner.

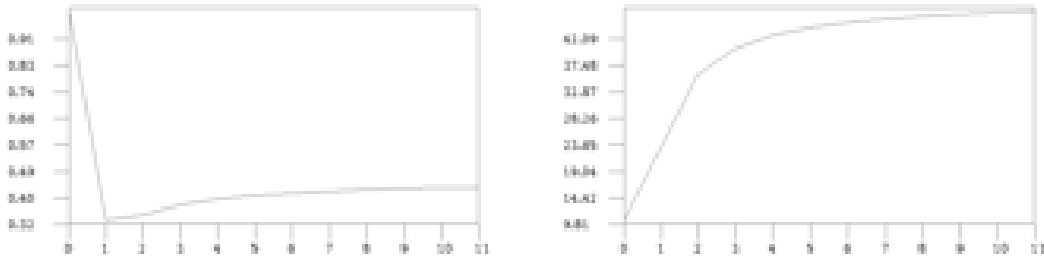


(a)  $E_x$  by analytical solution

(b)  $E_x$  by FDTD

Figure 12:  $E_x$  by the analytical solution and by FDTD simulation (case study 2).

Figure 12a shows snapshots of  $E_x(x + \Delta_s/2, y, z, \theta)$  calculated by the analytical formulas, while Figure 2b presents the corresponding results from the FDTD simulation. They are quite similar with some differences.



(a) Max difference vs step sizes

(b) Sum of difference vs step sizes

Figure 13: Effects of step sizes on FDTD simulations (Case-study 2).

Figure 13a shows the maximum difference between  $E_x$  values computed from the analytical solution and those obtained from FDTD simulations, while Figure 13b shows the cumulative absolute difference. These figures lead to the following observations:

- Reducing the step size to  $\Delta_s/2$  leads to a decrease in the maximum difference. Further reduction of the step size results in a slight increase in the maximum difference, indicating a weak non-monotonic trend.
- Reducing the step size to  $\Delta_s/2$  increases the cumulative difference. Further reduction of the step size produces only minor changes.

A similar weak non-monotonic behavior in the maximum difference is observed in a subset of the case studies, while the overall trend remains relatively flat. The origin of this behavior is not fully understood and warrants further investigation.

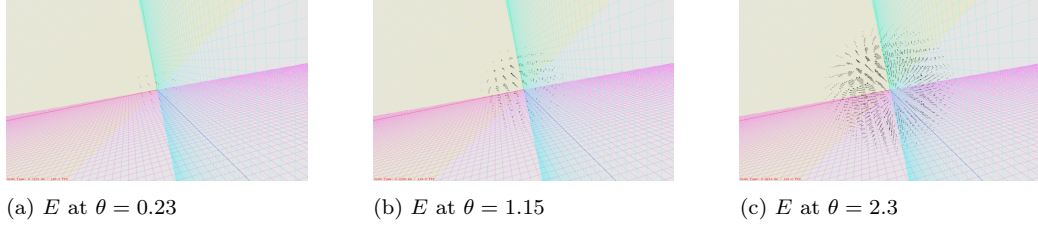


Figure 14: Electric field by analytical solution.  $q = 1, 5, 10$  (Case-study 2).

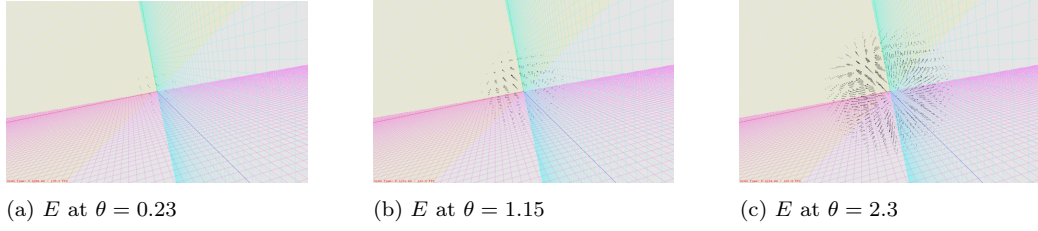


Figure 15: Electric field by FDTD.  $q = 1, 5, 10$  (Case-study 2).

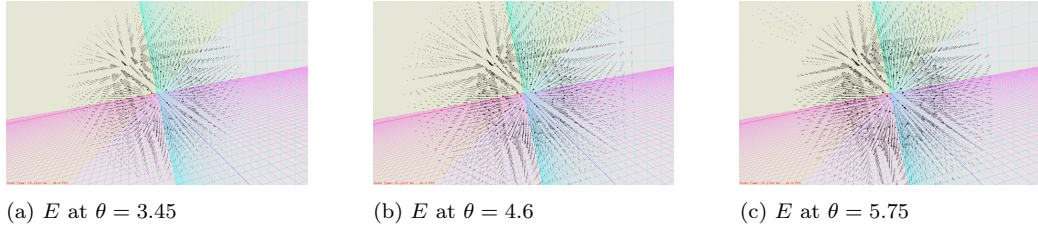


Figure 16: Electric field by analytical solution.  $q = 15, 20, 25$  (Case-study 2).

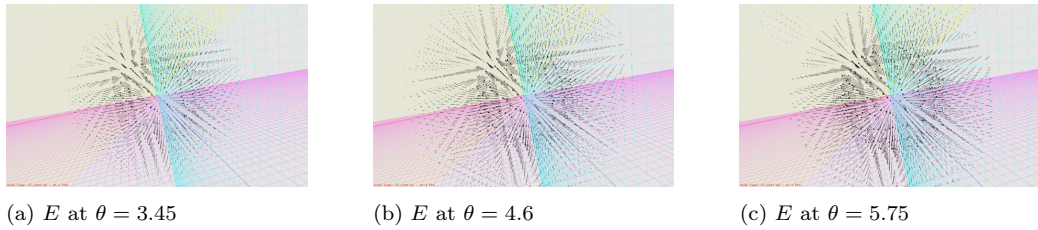


Figure 17: Electric field by FDTD.  $q = 15, 20, 25$  (Case-study 2).

Figures 14 and 16 show six snapshots of the electric field obtained from the analytical solution, while Figures 18 and 20 present the corresponding magnetic field snapshots. Figures 15, 17, 19, and 21 show the FDTD simulation results.

These three-dimensional visualizations exhibit close agreement between the analytical and FDTD results for this case, demonstrating the effectiveness of the FDTD method in capturing the field structure.

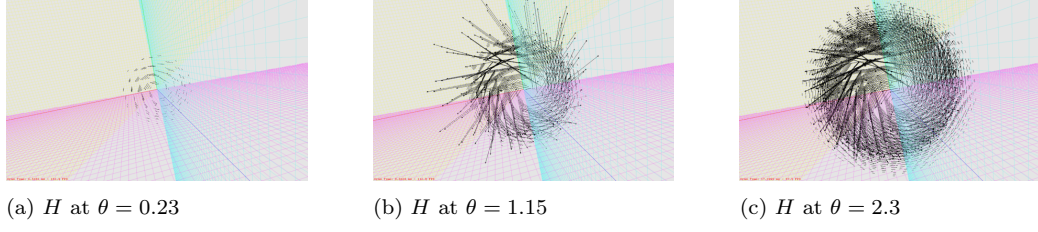


Figure 18: Magnetic field by analytical solution.  $q = 1, 5, 10$  (Case-study 2).

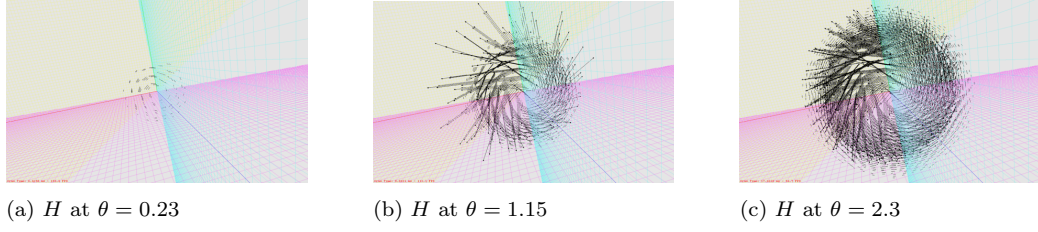


Figure 19: Magnetic field by FDTD.  $q = 1, 5, 10$  (Case-study 2).

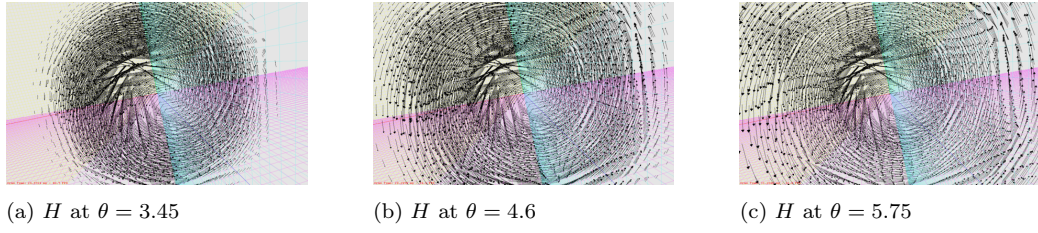


Figure 20: Magnetic field by analytical solution.  $q = 15, 20, 25$  (Case-study 2).

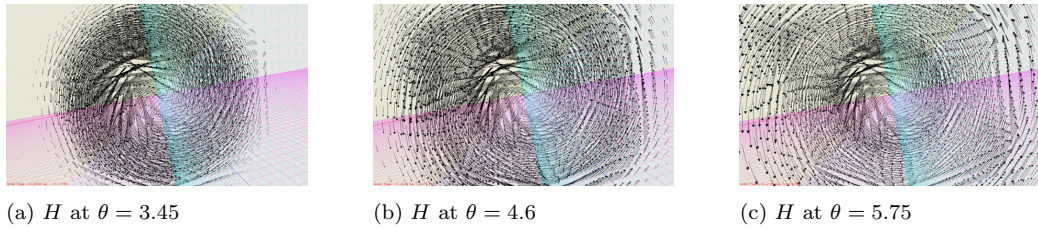


Figure 21: Magnetic field by FDTD.  $q = 15, 20, 25$  (Case-study 2).

### 4.3. Case-study 3: harmonic source

The following harmonic source [3] is used.

$$J(x, y, z, \theta) = \exp(-ar^2) \cos(\omega\theta) \vec{z} \quad (30)$$

where  $a, \omega \in \mathbb{R}_{>0}$  are constant.

The temporary derivatives of the source are

$$\frac{\partial^{2n} \cos(\omega\theta)}{\partial\theta^{2n}} = (-1)^n \omega^{2n} \cos(\omega\theta) \quad (31)$$

$$\frac{\partial^{2n+1} \cos(\omega\theta)}{\partial\theta^{2n+1}} = (-1)^{n+1} \omega^{2n+1} \sin(\omega\theta) \quad (32)$$

By applying (31), (32), (B.55) and (B.56) to (30) and substituting the results into (18) and (19), we obtain the following closed-form analytical solution:

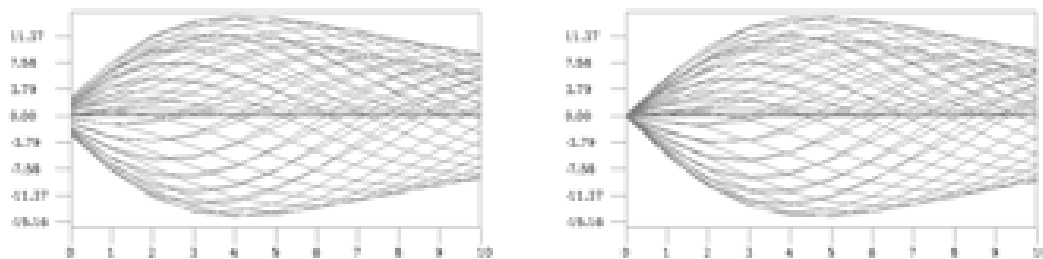
$$H(x, y, z, \theta) = -\frac{1}{a} \exp(-ar^2) \text{cosp}(\xi, \sigma, \omega_a)_{1,1} \vec{h} \quad (33)$$

$$E(x, y, z, \theta) = \frac{2\eta}{\sqrt{a}} \exp(-ar^2) \text{sinp}(\xi, \sigma, \omega_a)_{2,1} \vec{e} - \frac{\eta}{\sqrt{a}} \exp(-ar^2) f_z(\xi, \sigma, \omega_a) \vec{z} \quad (34)$$

$$f_z(\xi, \sigma, \omega_a) = \frac{\sin(\omega_a \xi)}{\omega_a} - 4 \text{sinp}(\xi, \sigma, \omega_a)_{1,1} + \sigma^2 \text{sinp}(\xi, \sigma, \omega_a)_{2,1}$$

where  $\xi = \sqrt{a}\theta$ ,  $\sigma = 2\sqrt{a}r$ ,  $\omega_a = \omega/\sqrt{a}$ .

Similar analytical insights can be obtained from the above solution formulas as in Case Study 2.



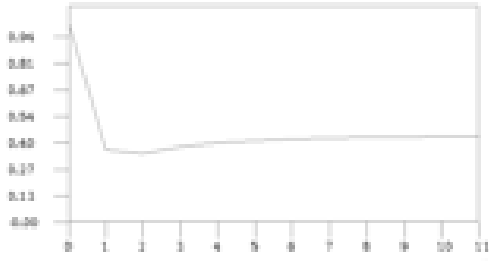
(a)  $E_x$  by analytical solution

(b)  $E_x$  by FDTD

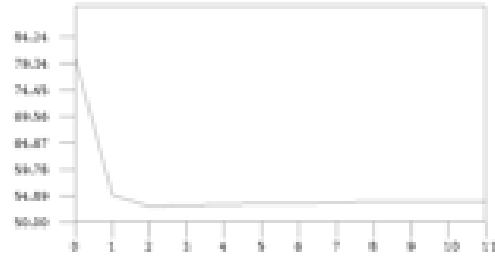
Figure 22:  $E_x$  by the analytical solution and by FDTD simulation (case study 3).

Figure 22a presents snapshots of  $E_x(x + \Delta_s/2, y, z, \theta)$  evaluated by the analytical formulas, while Figure 22b shows the corresponding results from FDTD simulation. They are quite similar with some differences.

Figure 23a shows the maximum difference between  $E_x$  values computed from the analytical solution and those obtained from FDTD simulations, while Figure 23b shows the cumulative difference. These figures lead to the following observations:

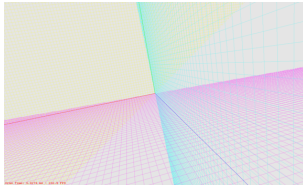


(a) Max difference vs step sizes

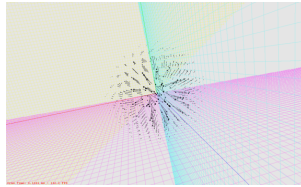


(b) Sum of difference vs step sizes

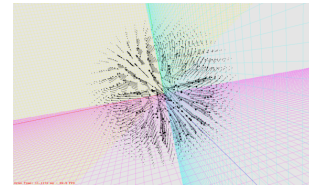
Figure 23: Effects of step sizes on FDTD simulations (Case-study 3).



(a)  $E$  at  $\theta = 0.23$

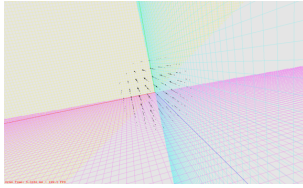


(b)  $E$  at  $\theta = 1.15$

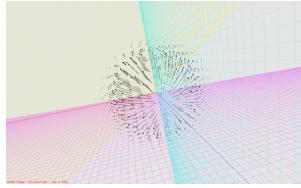


(c)  $E$  at  $\theta = 2.3$

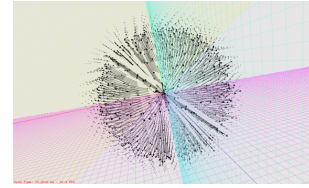
Figure 24: Electric field by analytical solution.  $q = 1, 5, 10$  (Case-study 3).



(a)  $E$  at  $\theta = 0.23$

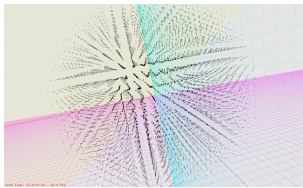


(b)  $E$  at  $\theta = 1.15$

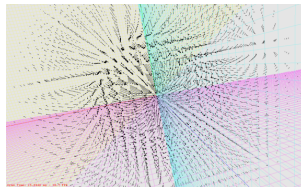


(c)  $E$  at  $\theta = 2.3$

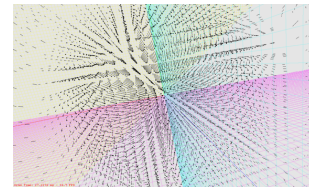
Figure 25: Electric field by FDTD.  $q = 1, 5, 10$  (Case-study 3).



(a)  $E$  at  $\theta = 3.45$



(b)  $E$  at  $\theta = 4.6$



(c)  $E$  at  $\theta = 5.75$

Figure 26: Electric field by analytical solution.  $q = 15, 20, 25$  (Case-study 3).

- Reducing the step size to  $\Delta_s/2$  leads to a decrease in the maximum difference. Further reduction of the step size results in negligible changes, with only a slight increase in the value.

- Reducing the step size to  $\Delta_s/2$  also decreases the cumulative difference. Further reduction of the step size produces negligible changes, and the values remain essentially constant.

These trends indicate that further reduction of the step size yields limited improvement in FDTD accuracy once the step size becomes sufficiently small.

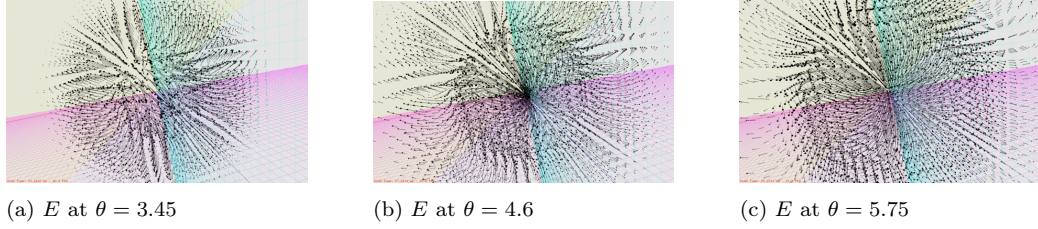


Figure 27: Electric field by FDTD.  $q = 15, 20, 25$  (Case-study 3).

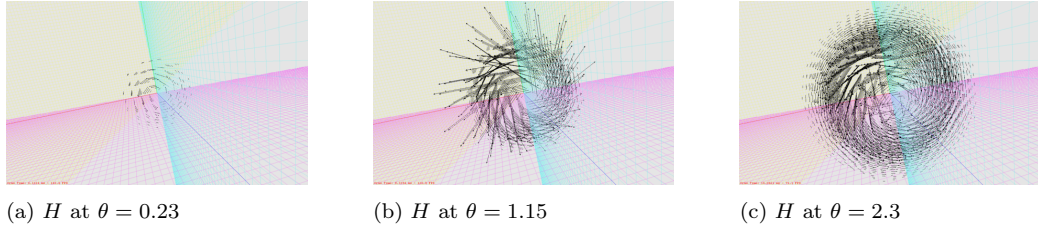


Figure 28: Magnetic field by analytical solution.  $q = 1, 5, 10$  (Case-study 3).

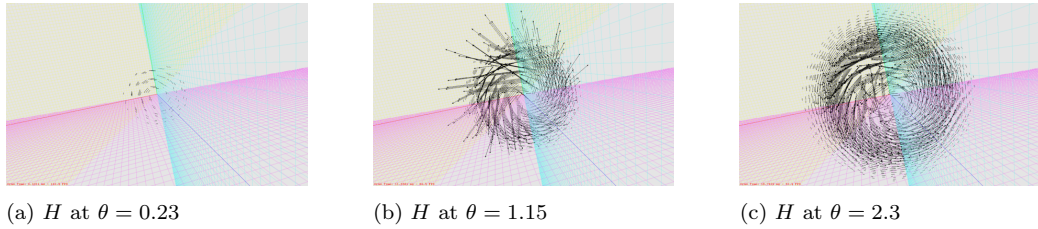


Figure 29: Magnetic field by FDTD.  $q = 1, 5, 10$  (Case-study 3).

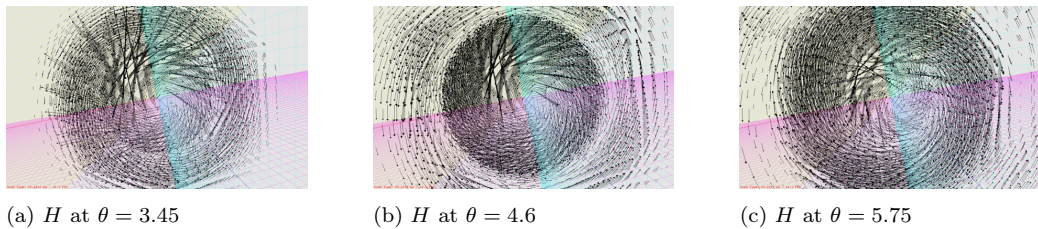


Figure 30: Magnetic field by analytical solution.  $q = 15, 20, 25$  (Case-study 3).

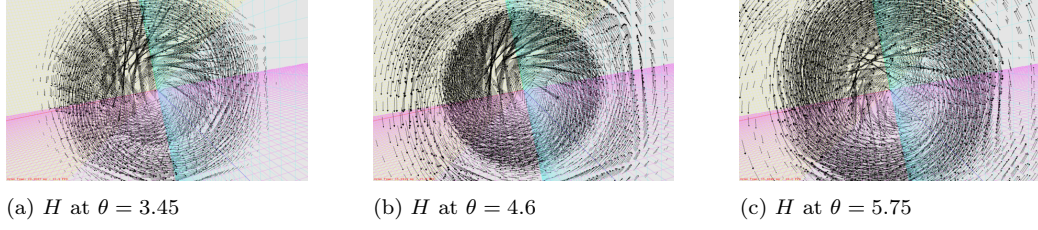


Figure 31: Magnetic field by FDTD.  $q = 15, 20, 25$  (Case-study 3).

Figures 24 and 26 show six snapshots of the electric field obtained from the analytical solution, while Figures 28 and 30 present the corresponding magnetic field snapshots. Figures 25, 27, 29, and 31 show the FDTD simulation results.

These three-dimensional visualizations exhibit close agreement between the analytical and FDTD results, indicating that the FDTD method effectively captures the field structure in this case.

#### 4.4. Case-study 4: Ricker wavelet source

The Ricker source [3] is given by

$$f_r(t) = (1 - 2(\pi f_p(t - d_r))^2) \exp(-(\pi f_p(t - d_r))^2)$$

where  $f_p$  is the "peak frequency" and  $d_r$  is the temporal delay.

Let

$$\begin{aligned} \theta &= ct \\ \theta_d &= cd_r \\ b &= \left( \frac{\pi f_p}{c} \right)^2 \end{aligned}$$

The source term becomes

$$J(x, y, z, \theta) = \exp(-ax^2)(1 - 2b(\theta - \theta_d)^2) \exp(-b(\theta - \theta_d)^2) \vec{z} \quad (35)$$

where  $a, b, \theta_d \in \mathbb{R}_{>0}$  are three constants.

Notice that (35) can be written as

$$J(x, y, z, \theta) = -\frac{1}{2b} \exp(-ax^2) \frac{\partial^2 \exp(-b(\theta - \theta_d)^2)}{\partial \theta^2} \vec{z} \quad (36)$$

Apply formulas (A.9) and (A.10) in [15] to (36), we have the temporal derivatives of the source:

$$\begin{aligned} & \frac{\partial^{2n} J(x, y, z, 0)}{\partial \theta^{2n}} \\ &= \frac{1}{2} \exp(-b\theta_d^2) (-1)^n b^n \sum_{k=0}^{n+1} (-1)^k q_{0,n+1,k} (2\sqrt{b}\theta_d)^{2k} \exp(-ar^2) \vec{z} \end{aligned} \quad (37)$$

$$\begin{aligned} & \frac{\partial^{2n+1} J(x, y, z, 0)}{\partial \theta^{2n+1}} \\ &= \frac{1}{2} \exp(-b\theta_d^2) (-1)^{n+1} \sqrt{b}^{2n+1} \sum_{k=0}^{n+1} (-1)^k p_{0,n+1,k} (2\sqrt{b}\theta_d)^{2k+1} \exp(-ar^2) \vec{z} \end{aligned} \quad (38)$$

By applying (37), (38), (B.55) and (B.56) to (36) and substituting the results into (18) and (19), we obtain the following closed-form analytical solution:

$$H(x, y, z, \theta) = \exp(-ar^2 - b\theta_d^2) f_h(\xi, \sigma, \xi_d, a_b) \vec{h} \quad (39)$$

$$E(x, y, z, \theta) = \frac{\eta}{\sqrt{b}} \exp(-ar^2 - b\theta_d^2) (f_z(\xi, \sigma, \xi_d, a_b) \vec{z} + f_e(\xi, \sigma, \xi_d, a_b) \vec{e}) \quad (40)$$

where  $\xi = \sqrt{b}\theta$ ,  $\xi_d = \sqrt{b}\theta_d$ ,  $\sigma = 2\sqrt{a}r$ ,  $a_b = a/b$ . Functions  $f_h$ ,  $f_z$  and  $f_e$  are given by

$$f_h(\xi, \sigma, \phi, \omega) = \frac{1}{2b} (\text{sinpo}(\xi, \sigma, \phi, \omega)_{1,1} - \text{cospe}(\xi, \sigma, \phi, \omega)_{1,1}) \quad (41)$$

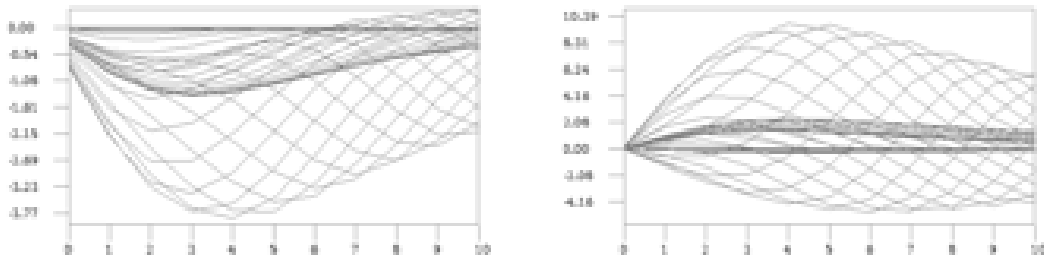
$$f_e(\xi, \sigma, \phi, \omega) = \frac{a}{b} (\text{sinpe}(\xi, \sigma, \phi, \omega)_{2,1} - \text{cospo}(\xi, \sigma, \phi, \omega)_{2,2}) \quad (42)$$

$$\begin{aligned} f_z(\xi, \sigma, \phi, \omega) &= \frac{1}{2} f_\xi(\xi, \phi) \\ &+ \frac{a}{2b} \sigma^2 \text{cospo}(\xi, \sigma, \phi, \omega)_{2,2} - \frac{2a}{b} \text{cospo}(\xi, \sigma, \phi, \omega)_{1,2} \\ &+ \frac{2a}{b} \text{sinpe}(\xi, \sigma, \phi, \omega)_{1,1} - \frac{a}{2b} \sigma^2 \text{sinpe}(\xi, \sigma, \phi, \omega)_{2,1} \end{aligned} \quad (43)$$

where

$$\begin{aligned} f_\xi(\xi, \phi) &= 2\phi(3 - 2\phi^2)\xi^2 - 2(1 - 2\phi^2)\xi \\ &- 2\phi \text{cosp}(\xi, 2\phi)_{0,2,2} + \text{sinq}(\xi, 2\phi)_{0,1,2} \end{aligned} \quad (44)$$

Similar analytical insights can be obtained from the above solution formulas, as demonstrated in Case Study 2.



(a)  $E_x$  by analytical solution

(b)  $E_x$  by FDTD

Figure 32:  $E_x$  by the analytical solution and by FDTD simulation (case study 4).

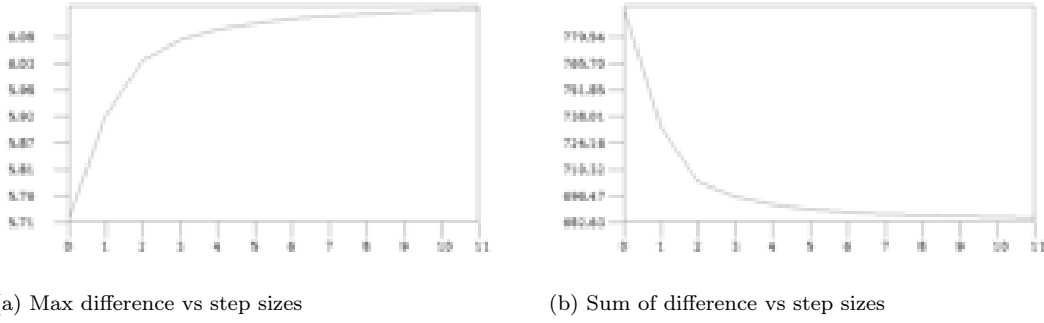


Figure 33: Effects of step sizes on FDTD simulations (Case-study 4).

Figure 32a shows snapshots of  $E_x(x + \Delta_s/2, y, z, \theta)$  evaluated using the analytical formulas, while Figure 32b presents the corresponding results from the FDTD simulation. The  $E_x$  values exhibit significant differences between the two approaches, even though the corresponding three-dimensional visualizations show close agreement in the overall field structure.

Figure 33a shows the maximum difference between  $E_x$  values computed from the analytical solution and those obtained from FDTD simulations, while Figure 33b shows the cumulative difference. These figures exhibit the same trend observed in the other cases: the FDTD results become largely insensitive to further step size reduction once the step size becomes sufficiently small.

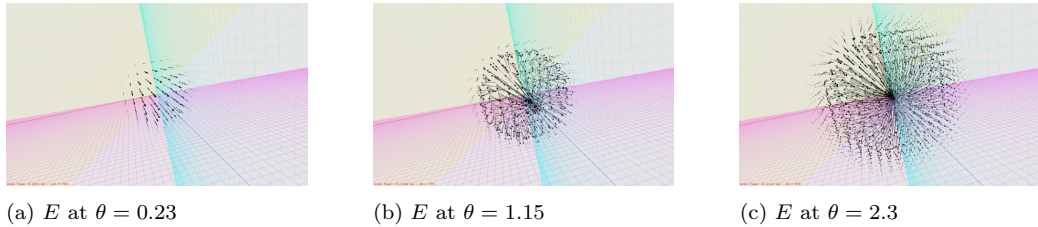


Figure 34: Electric field by analytical solution.  $q = 1, 5, 10$  (Case-study 4).

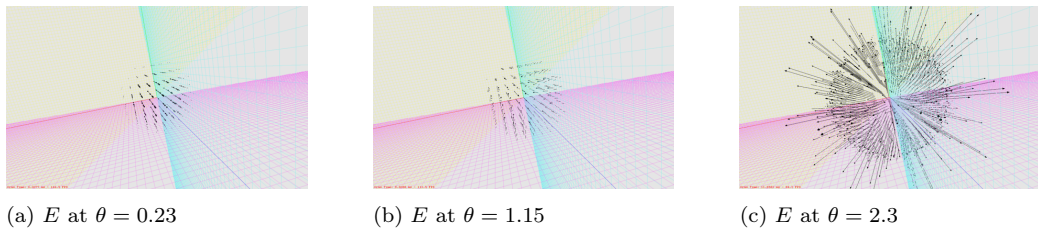


Figure 35: Electric field by FDTD.  $q = 1, 5, 10$  (Case-study 4).

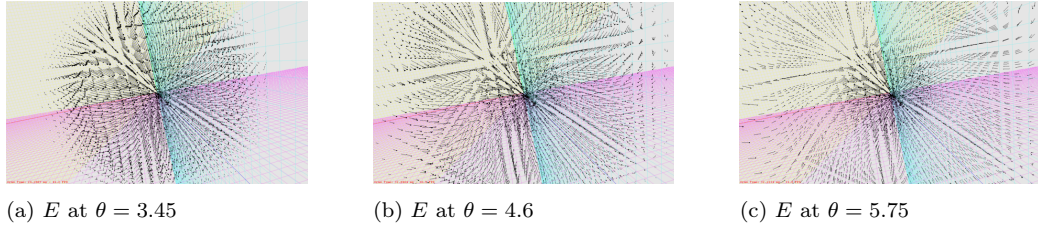


Figure 36: Electric field by analytical solution.  $q = 15, 20, 25$  (Case-study 4).

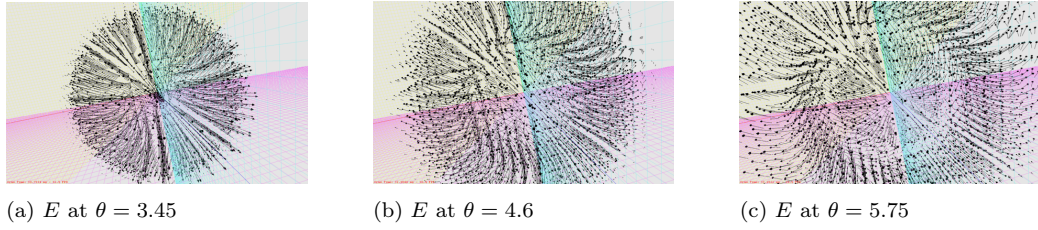


Figure 37: Electric field by FDTD.  $q = 15, 20, 25$  (Case-study 4).

Figures 34 and 36 show six snapshots of the electric field obtained from the analytical solution, while Figures 38 and 40 present the corresponding magnetic field snapshots. Figures 35, 37, 39, and 41 show the FDTD simulation results.

These three-dimensional visualizations demonstrate close agreement between the analytical and FDTD results, indicating that the FDTD method effectively captures the field structure in this case.

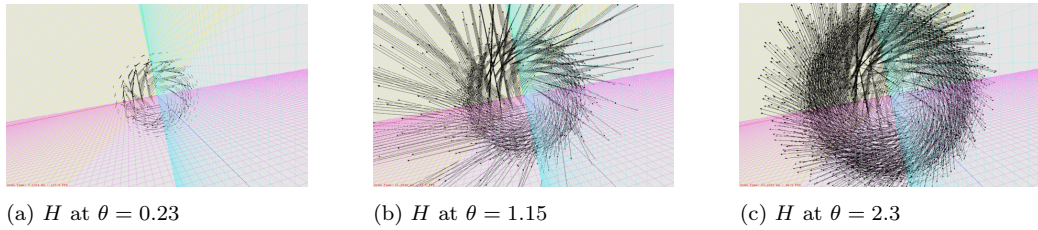


Figure 38: Magnetic field by analytical solution.  $q = 1, 5, 10$  (Case-study 4).

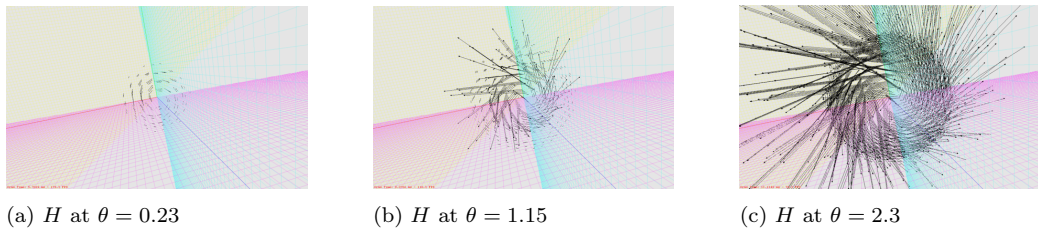


Figure 39: Magnetic field by FDTD.  $q = 1, 5, 10$  (Case-study 4).

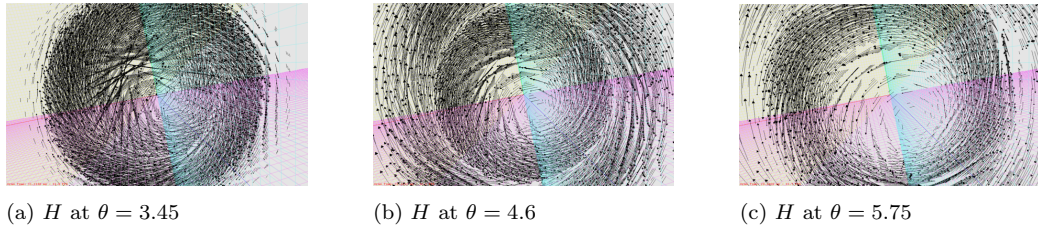


Figure 40: Magnetic field by analytical solution.  $q = 15, 20, 25$  (Case-study 4).

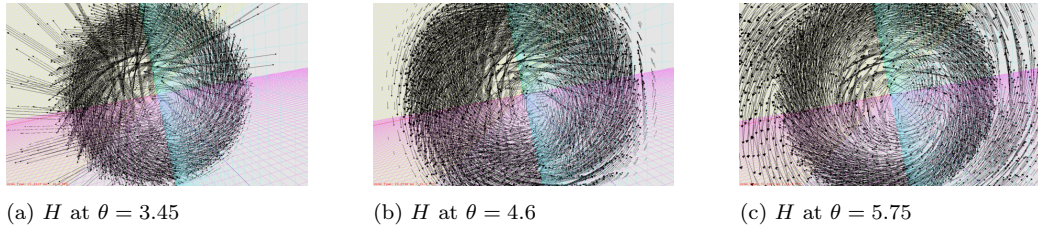


Figure 41: Magnetic field by FDTD.  $q = 15, 20, 25$  (Case-study 4).

## 5. Discussion

The present work constructs a generic solution to Maxwell's equations using an infinite-order curl-operator expansion. This approach yields what we term an analytical solution, in contrast to conventional numerical schemes. In the case studies, the differential operators appearing in the general expressions are explicitly evaluated, leading to formulas that we refer to as closed-form analytical solutions.

These closed-form solutions reveal that the electromagnetic fields travel in deformed sine and cosine functions; the structures of deformations depend on the initial conditions and source terms. To illustrate the nature of this deformation, consider the classical traveling-wave sine function, which admits the series representation

$$\sin(x - ct) = \sum_{n=0}^{\infty} \frac{(-1)^n (x - ct)^{2n+1}}{(2n + 1)!}$$

Within the present framework, a representative deformed sine function takes the form

$$\sum_{n=0}^{\infty} \frac{(-1)^n (ct)^{2(n+s)+1}}{(2(n + s) + 1)!} \sum_{k=0}^n p_{2,n,k} (2x)^{2k}$$

where  $p_{2,n,k}$  are coefficients determined by the operator expansion and  $s$  is a parameter arising from the solution construction. In contrast to the classical case, the spatial and temporal variables are no longer coupled through a simple phase

term  $(x - ct)$ ; instead, the solution exhibits a structured mixing of spatial polynomials and temporally weighted series terms. Many other deformations arise naturally within the same analytical framework. This structural shift suggests that the classical notion of phase velocity may require reinterpretation upon this revelation.

The deformed trigonometric functions describe the instantaneous behavior of the electromagnetic fields. Understanding their implications for steady-state or long-time behavior requires analysis of their asymptotic properties as spatial and temporal variables approach infinity. In particular, it remains an open question whether the deformation diminishes in these limits, potentially recovering standard trigonometric behavior.

Notably, the deformed sine and cosine functions are not limited to specific case studies but are intrinsically embedded in the general solution formulas (16), (17), (18) and (19). This suggests that, within the present analytical framework, the evolution of electromagnetic fields can be interpreted as being governed by these deformed trigonometric structures, whose forms are determined by the initial conditions and source terms. This observation reveals a unifying structural feature of the analytical solutions and provides a new perspective on how electromagnetic fields propagate under general conditions.

Unlike classical periodic functions, whose values can be readily evaluated for arbitrarily large arguments, the deformed sine and cosine functions are not strictly periodic. This lack of exact periodicity introduces additional challenges in evaluating the solutions for large spatial or temporal domains. Developing efficient analytical or numerical methods for their evaluation in such regimes represents a significant direction for future research in applied mathematics.

The Time-Space theorem presented in Appendix A can also be applied to higher-order FDTD simulations. The author has implemented such schemes using both the Yee grid and a non-staggered grid, and in both cases the expected improvements in accuracy were observed.

## 6. Conclusion

This work presents an operator-based framework for constructing analytical solutions to Maxwell's equations in open-space settings with general initial conditions and source terms. The resulting infinite-order curl-operator expansion provides explicit function-to-function mappings and leads to closed-form representations in terms of deformed sine and cosine functions. Comparisons with Yee FDTD simulations demonstrate both agreement in field structure and systematic differences attributable to discretization effects. The observed insensitivity of FDTD results to further step size reduction highlights inherent limitations of numerical refinement. Beyond validation, the analytical solutions offer new theoretical insight

into electromagnetic field behavior and serve as practical benchmarks for computational electromagnetics. Future work will further investigate the properties of the deformed functions and extend the framework to broader classes of problems.

## Appendix A. Time-Space theorem

Maxwell's equations establish a correspondence between first-order temporal derivatives and first-order spatial curls. The following theorem generalizes this relationship to derivatives of arbitrary order, providing a systematic extension of the time-space structure.

**Theorem 5.** *If a function-pair  $H(x, y, z, \theta), E(x, y, z, \theta) \in C^\infty(\mathbb{R}^4, \mathbb{R}^3)$  satisfies Maxwell's equations (1) and (2) then for any  $n \geq 0$*

$$\frac{\partial^{2n+1} H}{\partial \theta^{2n+1}} = \frac{1}{\eta} (-1)^{n+1} \nabla^{2n+1} \times E + J_{h,2n+1} \quad (\text{A.1})$$

$$\frac{\partial^{2n+2} H}{\partial \theta^{2n+2}} = (-1)^{n+1} \nabla^{2n+2} \times H + J_{h,2n+2} \quad (\text{A.2})$$

$$\frac{\partial^{2n+1} E}{\partial \theta^{2n+1}} = \eta (-1)^n \nabla^{2n+1} \times H + \eta J_{e,2n+1} \quad (\text{A.3})$$

$$\frac{\partial^{2n+2} E}{\partial \theta^{2n+2}} = (-1)^{n+1} \nabla^{2n+2} \times E + \eta J_{e,2n+2} \quad (\text{A.4})$$

where the source terms are given by

$$J_{h,1} = 0$$

$$J_{h,2n+1} = \sum_{m=1}^n (-1)^{m+1} \nabla^{2m-1} \times \frac{\partial^{2(n-m)+1} J}{\partial \theta^{2(n-m)+1}}, n > 0 \quad (\text{A.5})$$

$$J_{h,2n+2} = \sum_{m=0}^n (-1)^m \nabla^{2m+1} \times \frac{\partial^{2(n-m)} J}{\partial \theta^{2(n-m)}} \quad (\text{A.6})$$

$$J_{e,2n+1} = \sum_{m=0}^n (-1)^{m+1} \nabla^{2m} \times \frac{\partial^{2(n-m)} J}{\partial \theta^{2(n-m)}} \quad (\text{A.7})$$

$$J_{e,2n+2} = \sum_{m=0}^n (-1)^{m+1} \nabla^{2m} \times \frac{\partial^{2(n-m)+1} J}{\partial \theta^{2(n-m)+1}} \quad (\text{A.8})$$

*Proof.* We will induct on  $n$ .

**Base case** ( $n = 0, n = 1$ ): It is easy to validate that for  $n = 0$  and  $n = 1$  the theorem holds.

**Inductive Hypothesis** ( $n = m$ ): Assume for some  $m \in \mathbb{Z}_{\geq 0}$  the theorem holds.

**Inductive Step:**

By applying the differential operation  $\partial/\partial\theta$  on both sides of (A.2) with  $n = m$ , we have

$$\frac{\partial^{2(m+1)+1} H}{\partial\theta^{2(m+1)+1}} = \frac{1}{\eta} (-1)^{(m+1)+1} \nabla^{2(m+1)+1} \times E + \sum_{k=1}^{m+1} (-1)^{k+1} \nabla^{2k-1} \times \frac{\partial^{2(m+1-k)+1} J}{\partial\theta^{2(m+1-k)+1}} \quad (\text{A.9})$$

The above shows that (A.1) holds for  $n = m + 1$ .

By applying the differential operation  $\partial/\partial\theta$  on both sides of (A.9) and substitute (2) into it, we have

$$\frac{\partial^{2(m+2)} H}{\partial\theta^{2(m+2)}} = (-1)^{m+2} \nabla^{2(m+2)} \times H + \sum_{k=0}^{m+1} (-1)^k \nabla^{2k+1} \times \frac{\partial^{2(m+1-k)} J}{\partial\theta^{2(m+1-k)}}$$

The above shows that (A.2) holds for  $n = m + 1$ .

By applying the differential operation  $\partial/\partial\theta$  on both sides of (A.4) with  $n = m$  and substitute (2) into it, we have

$$\frac{\partial^{2(m+1)+1} E}{\partial\theta^{2(m+1)+1}} = \eta (-1)^{m+1} \nabla^{2(m+1)+1} \times H + \eta \sum_{k=0}^{m+1} (-1)^{k+1} \nabla^{2k} \times \frac{\partial^{2(m+1-k)} J}{\partial\theta^{2(m+1-k)}} \quad (\text{A.10})$$

The above shows that (A.3) holds for  $n = m + 1$ .

By applying the differential operation  $\partial/\partial\theta$  on both sides of (A.10) and substitute (1) into it, we have

$$\frac{\partial^{2(m+1+1)} E}{\partial\theta^{2(m+1+1)}} = (-1)^{m+1+1} \nabla^{2(m+1+1)} \times E + \eta \sum_{k=0}^{m+1} (-1)^{k+1} \nabla^{2k} \times \frac{\partial^{2(m+1-k)+1} J}{\partial\theta^{2(m+1-k)+1}}$$

The above shows that (A.4) holds for  $n = m + 1$ .

$\therefore$  By the principle of induction, (A.1), (A.2), (A.3) and (A.4) hold for all  $n \in \mathbb{Z}_{\geq 0}$ .  $\square$

## Appendix B. Formulas used by the case-studies

To apply the extended Taylor series presented in this paper, one must obtain analytical expressions for the derivatives and curls of the initial values and the source term. For the case studies presented in this paper, the required formulas are provided and proved in this appendix.

*Appendix B.1. Definitions*

For three integers,  $h, n$  and  $k$ ,  $h \geq 0, n \geq 0$ , the following two coefficients play key roles in forming deformed sine and cosine functions:

$$p_{h,n,k} := \frac{n!(k+h)!(2(n+h)+1)!}{(n-k)!k!(n+h)!(2(k+h)+1)!} \quad (\text{B.1})$$

$$p_{h,n,k} := 0, \quad \text{if } k < 0 \vee k > n$$

$$q_{h,n,k} := \frac{(n+1)!(k+1+h)!(2(n+h))!}{(n-k)!(k+1)!(n+1+h)!(2(k+h))!} \quad (\text{B.2})$$

$$h \geq 0, n \geq 0, n \geq k \geq 0$$

Some commonly used vector variables:

$$\vec{s} = \begin{bmatrix} x \\ y \\ z \end{bmatrix} \quad (\text{B.3})$$

$$\vec{z} = \begin{bmatrix} 0 \\ 0 \\ 1 \end{bmatrix} \quad (\text{B.4})$$

$$\vec{b} = \begin{bmatrix} yz \\ -2zx \\ xy \end{bmatrix} \quad (\text{B.5})$$

$$\vec{c} = \begin{bmatrix} x \\ 0 \\ -z \end{bmatrix} \quad (\text{B.6})$$

$$\vec{f} = \begin{bmatrix} y \\ -x \\ 0 \end{bmatrix} \quad (\text{B.7})$$

When we are handling Gaussian function  $\exp(-ar^2)$  the following values frequently appear. They are defined below and used throughout this report.

$$a \in \mathbb{R}_{>0} \quad (\text{B.8})$$

$$r^2 = x^2 + y^2 + z^2 \quad (\text{B.9})$$

$$g = 2a \quad (\text{B.10})$$

$$w = gr^2 \quad (\text{B.11})$$

$$\vec{d} = g(x^2 - z^2)\vec{s} \quad (\text{B.12})$$

$$\vec{h} = g\vec{f} \quad (\text{B.13})$$

$$\vec{e} = gz\vec{s} \quad (\text{B.14})$$

Appendix B.2. *Deformed sine and cosine functions*

$$\text{cosp}(\xi, \sigma)_{h,s,d} = \sum_{n=0}^{\infty} \frac{(-1)^n \xi^{2(n+s)}}{(2(n+s))!} \sum_{k=0}^{n+d} (-1)^k p_{h+d,n,k} \sigma^{2k} \quad (\text{B.15})$$

$$\text{sinp}(\xi, \sigma)_{h,s,d} = \sum_{n=0}^{\infty} \frac{(-1)^n \xi^{2(n+s)+1}}{(2(n+s)+1)!} \sum_{k=0}^{n+d} (-1)^k p_{h+d,n,k} \sigma^{2k} \quad (\text{B.16})$$

$$\text{cosq}(\xi, \sigma)_{h,s,d} = \sum_{n=0}^{\infty} \frac{(-1)^n \xi^{2(n+s)}}{(2(n+s))!} \sum_{k=0}^{n+d} (-1)^k q_{h+d,n,k} \sigma^{2k} \quad (\text{B.17})$$

$$\text{sinq}(\xi, \sigma)_{h,s,d} = \sum_{n=0}^{\infty} \frac{(-1)^n \xi^{2(n+s)+1}}{(2(n+s)+1)!} \sum_{k=0}^{n+d} (-1)^k q_{h+d,n,k} \sigma^{2k} \quad (\text{B.18})$$

$$\text{cosp}(\xi, \sigma, \omega)_{h,s} = \sum_{n=0}^{\infty} \frac{(-1)^n \xi^{2(n+s)}}{(2(n+s))!} \sum_{m=0}^n \omega^{2(n-m)} \sum_{k=0}^m (-1)^k p_{h,m,k} \sigma^{2k} \quad (\text{B.19})$$

$$\text{sinp}(\xi, \sigma, \omega)_{h,s} = \sum_{n=0}^{\infty} \frac{(-1)^n \xi^{2(n+s)+1}}{(2(n+s)+1)!} \sum_{m=0}^n \omega^{2(n-m)} \sum_{k=0}^m (-1)^k p_{h,m,k} \sigma^{2k} \quad (\text{B.20})$$

$$\text{cospo}(\xi, \sigma, \phi, \omega)_{h,s} = \sum_{n=0}^{\infty} \frac{(-1)^n \xi^{2(n+s)}}{(2(n+s))!} \sum_{m=0}^n f_{o,n-m}(\phi) \omega^m \sum_{k=0}^m (-1)^k p_{h,m,k} \sigma^{2k} \quad (\text{B.21})$$

$$\text{cospe}(\xi, \sigma, \phi, \omega)_{h,s} = \sum_{n=0}^{\infty} \frac{(-1)^n \xi^{2(n+s)}}{(2(n+s))!} \sum_{m=0}^n f_{e,n-m}(\phi) \omega^m \sum_{k=0}^m (-1)^k p_{h,m,k} \sigma^{2k} \quad (\text{B.22})$$

$$\text{sinpo}(\xi, \sigma, \phi, \omega)_{h,s} = \sum_{n=0}^{\infty} \frac{(-1)^n \xi^{2(n+s)+1}}{(2(n+s)+1)!} \sum_{m=0}^n f_{o,n-m}(\phi) \omega^m \sum_{k=0}^m (-1)^k p_{h,m,k} \sigma^{2k} \quad (\text{B.23})$$

$$\text{sinpe}(\xi, \sigma, \phi, \omega)_{h,s} = \sum_{n=0}^{\infty} \frac{(-1)^n \xi^{2(n+s)+1}}{(2(n+s)+1)!} \sum_{m=0}^n f_{e,n-m}(\phi) \omega^m \sum_{k=0}^m (-1)^k p_{h,m,k} \sigma^{2k} \quad (\text{B.24})$$

where functions  $f_{o,n}(\phi)$  and  $f_{e,n}(\phi)$  are defined by

$$f_{o,n}(\phi) = \sum_{k=0}^{n+1} (-1)^k p_{0,n+1,k} (2\phi)^{2k+1} \quad (\text{B.25})$$

$$f_{e,n}(\phi) = \sum_{k=0}^{n+1} (-1)^k q_{0,n+1,k} (2\phi)^{2k} \quad (\text{B.26})$$

### Appendix B.3. Identities

**Lemma 6.** For  $n \geq 0, n \geq k \geq 0$  we have the following identities

$$p_{h,n,n} = 1 \quad (\text{B.27})$$

$$p_{2,n,k} = p_{1,n,k} + 4(k+1)p_{1,n,k+1} \quad (\text{B.28})$$

$$p_{3,n,k} = 4(k+1)p_{2,n,k+1} + p_{2,n,k} \quad (\text{B.29})$$

$$p_{1,n+1,k} = 2(2k+5)p_{2,n,k} + p_{2,n,k-1} \quad (\text{B.30})$$

$$p_{1,n+1,k} - 4p_{2,n,k} = 2(2k+3)p_{2,n,k} + p_{2,n,k-1} \quad (\text{B.31})$$

$$p_{2,n+1,k} = 4(k+1)u_{n,k+1} + 4p_{3,n,k} + u_{n,k} \quad (\text{B.32})$$

where

$$u_{n,k} = p_{1,n+1,k} - 4p_{2,n,k} \quad (\text{B.33})$$

**Lemma 7.**

$$\sum_{k=0}^{n+1} \frac{(-1)^k}{2^{n+1-k}} (p_{2,n,k-1} + 4p_{1,n,k}) w^k = \sum_{k=0}^n \frac{(-1)^k}{2^{n-k}} (2p_{1,n,k} - wp_{2,n,k}) w^k \quad (\text{B.34})$$

where  $n \geq 0, w \in \mathbb{R}$ .

The above lemmas follow directly from (B.1); their proofs are omitted. (B.31) and (B.33) give

$$u_{n,k} = 2(2k+3)p_{2,n,k} + p_{2,n,k-1} \quad (\text{B.35})$$

**Lemma 8.**

$$\nabla \times \vec{b} = 3\vec{c} \quad (\text{B.36})$$

$$\nabla \times w^k \vec{b} = (2k+3)w^k \vec{c} - 2kw^{k-1} \vec{d}; \forall k > 0 \quad (\text{B.37})$$

$$g\vec{s} \times \vec{b} = w\vec{c} - \vec{d} \quad (\text{B.38})$$

$$\nabla \times \vec{c} = 0 \quad (\text{B.39})$$

$$\nabla \times w^k \vec{c} = -2kgw^{k-1} \vec{b}; \forall k > 0 \quad (\text{B.40})$$

$$\nabla \times w^k \vec{d} = 2gw^k \vec{b}; \forall k \geq 0 \quad (\text{B.41})$$

$$\vec{s} \times \vec{d} = 0 \quad (\text{B.42})$$

$$\vec{s} \times \vec{c} = -\vec{b} \quad (\text{B.43})$$

$$\nabla \times \vec{h} = -2g\vec{z} \quad (\text{B.44})$$

$$\nabla \times w^k \vec{h} = -2g(k+1)w^k \vec{z} + 2gkw^{k-1} \vec{c}; k > 0 \quad (\text{B.45})$$

$$g\vec{s} \times \vec{h} = -gw\vec{z} + g\vec{c} \quad (\text{B.46})$$

$$\nabla \times \vec{z} = 0 \quad (\text{B.47})$$

$$\nabla \times w^k \vec{z} = 2kw^{k-1} \vec{h}, \forall k > 0 \quad (\text{B.48})$$

$$\nabla \times w^k \vec{e} = -w^k \vec{h}, \forall k \geq 0 \quad (\text{B.49})$$

$$g\vec{s} \times \vec{z} = \vec{h} \quad (\text{B.50})$$

$$g\vec{s} \times \vec{e} = 0 \quad (\text{B.51})$$

The proofs of the above formulas are straightforward and therefore omitted.

#### Appendix B.4. Theorems

All symbols not otherwise specified are defined in Appendix B.1.

**Theorem 9.** For all  $F \in C^\infty(\mathbb{R}^3, \mathbb{R}^3)$ ,

$$\nabla \times \exp(-ar^2)F = \exp(-ar^2)(\nabla - g\vec{s}) \times F \quad (\text{B.52})$$

The proof of (B.52) is straightforward and therefore omitted.

**Theorem 10.** For  $B = \exp(-ar^2)\vec{b}$ , the curls of  $B$  are given by

$$\nabla^{2n} \times B = \exp(-ar^2)g^n \sum_{k=0}^n \frac{(-1)^k}{2^{n-k}} p_{2,n,k} w^k \vec{b} \quad (\text{B.53})$$

$$\nabla^{2n+1} \times B = \exp(-ar^2)g^n \left( \sum_{k=0}^{n+1} \frac{(-1)^k}{2^{n+1-k}} u_{n,k} w^k \vec{c} + \sum_{k=0}^n \frac{(-1)^k}{2^{n-k}} p_{3,n,k} w^k \vec{d} \right) \quad (\text{B.54})$$

$\forall n \geq 0$

*Proof.* We will induct on  $n$ .

**Base case** ( $n = 0$ ): It is easy to see that for  $n = 0$  (B.53) and (B.54) hold.

**Inductive Hypothesis** ( $n = m$ ): Assume for some  $m \in \mathbb{Z}_{\geq 0}$  (B.53) holds.

**Inductive Step:** Let's first prove that (B.54) holds for  $n = m$ . Applying the curl operation on both side of (B.53) with  $n = m$  and using (B.52), we have

$$\begin{aligned} \nabla^{2m+1} \times B &= \nabla \times \exp(-ar^2)g^m \sum_{k=0}^m \frac{(-1)^k}{2^{m-k}} p_{2,m,k} w^k \vec{b} \\ &= \exp(-ar^2)g^m \left( \sum_{k=0}^m \frac{(-1)^k}{2^{m-k}} p_{2,m,k} \nabla \times w^k \vec{b} - \sum_{k=0}^m \frac{(-1)^k}{2^{m-k}} p_{2,m,k} w^k g\vec{s} \times \vec{b} \right) \end{aligned}$$

Apply (B.36), (B.37) and (B.38) and regroup the summations, we have

$$\begin{aligned} \nabla^{2m+1} \times B &= \exp(-ar^2)g^m \sum_{k=0}^{m+1} \frac{(-1)^k}{2^{m+1-k}} (2(2k+3)p_{2,m,k} + p_{2,m,k-1}) w^k \vec{c} \\ &\quad + \exp(-ar^2)g^m \sum_{k=0}^m \frac{(-1)^k}{2^{m-k}} (4(k+1)p_{2,m,k+1} + p_{2,m,k}) w^k \vec{d} \end{aligned}$$

By (B.35) and (B.29), we arrive at (B.54) with  $n = m$ .

Applying the curl operation on both side of (B.54) with  $n = m$  and using (B.52), we obtain

$$\begin{aligned} & \nabla^{2m+2} \times B \\ &= \exp(-ar^2)g^m \left( \sum_{k=0}^{m+1} \frac{(-1)^k}{2^{m+1-k}} u_{m,k} \nabla \times w^k \vec{c} + \sum_{k=0}^m \frac{(-1)^k}{2^{m-k}} p_{3,m,k} \nabla \times w^k \vec{d} \right) \\ & - \exp(-ar^2)g^m \left( \sum_{k=0}^{m+1} \frac{(-1)^k}{2^{m+1-k}} u_{m,k} w^k g \vec{s} \times \vec{c} + \sum_{k=0}^m \frac{(-1)^k}{2^{m-k}} p_{3,m,k} w^k g \vec{s} \times \vec{d} \right) \end{aligned}$$

By (B.39), (B.40), (B.41), (B.42) and (B.43), and regroup the summations, we have

$$\nabla^{2m+2} \times B = \exp(-ar^2)g^{m+1} \sum_{k=0}^{m+1} \frac{(-1)^k}{2^{m+1-k}} (4(k+1)u_{m,k+1} + 4p_{3,m,k} + u_{m,k}) w^k \vec{b}$$

By (B.32) we arrive at (B.53) with  $n = m + 1$ .

$\therefore$  By the principle of induction, (B.53) and (B.54) hold for all  $n \in \mathbb{Z}_{\geq 0}$ .  $\square$

**Theorem 11.** For  $B = \exp(-ar^2)\vec{z}$ , the curls of  $B$  are given by

$$\nabla^{2n+1} \times B = g^n \exp(-ar^2) \sum_{k=0}^n \frac{(-1)^{k+1}}{2^{n-k}} p_{1,n,k} w^k \vec{h} \quad (\text{B.55})$$

$$\begin{aligned} \nabla^{2(n+1)} \times B &= g^{n+1} \exp(-ar^2) \sum_{k=0}^n \frac{(-1)^k}{2^{n-k}} p_{2,n,k} w^k \vec{e} \\ &+ g^{n+1} \exp(-ar^2) \sum_{k=0}^n \frac{(-1)^k}{2^{n-k}} (2p_{1,n,k} - wp_{2,n,k}) w^k \vec{z} \\ &\quad \forall n \geq 0 \end{aligned} \quad (\text{B.56})$$

*Proof.* We will induct on  $n$ .

**Base case** ( $n = 0, n = 1$ ): It is easy to verify that for  $n = 0$  and  $n = 1$  (B.55) and (B.56) hold.

**Inductive Hypothesis** ( $n = m$ ): Assume for some  $m \in \mathbb{Z}_{>0}$  (B.55) holds.

**Inductive Step:** Let's first prove that (B.56) holds for  $n = m$ . Applying the curl operation on both sides of (B.55) with  $n = m$  and using (B.52), we have

$$\begin{aligned} \nabla^{2m+2} \times B &= g^m \exp(-ar^2) \sum_{k=0}^m \frac{(-1)^{k+1}}{2^{m-k}} p_{1,m,k} \nabla \times w^k \vec{h} \\ & - g^m \exp(-ar^2) \sum_{k=0}^m \frac{(-1)^{k+1}}{2^{m-k}} p_{1,m,k} w^k g \vec{s} \times \vec{h} \end{aligned}$$

Applying (B.44), (B.45) and (B.46), and moving the factor  $g^m \exp(-ar^2)$  to the left hand side for cleanness, the above equation can be written as

$$\begin{aligned}
& g^{-m} \exp(ar^2) \nabla^{2m+2} \times B = \\
& - \frac{1}{2^m} p_{1,m,0} (-2g\vec{z}) \\
& + \sum_{k=1}^m \frac{(-1)^{k+1}}{2^{m-k}} p_{1,m,k} (-2g(k+1)w^k\vec{z} + 2gkw^{k-1}\vec{e}) \\
& - \sum_{k=0}^m \frac{(-1)^{k+1}}{2^{m-k}} p_{1,m,k} w^k (-gw\vec{z} + g\vec{e})
\end{aligned}$$

The above can be rearranged into

$$\begin{aligned}
& g^{-(m+1)} \exp(ar^2) \nabla^{2m+2} \times B = \\
& \frac{2}{2^m} p_{1,m,0} \vec{z} + (-1)^{m+1} p_{1,m,m} w^{m+1} \vec{z} \\
& + \sum_{k=1}^m \frac{(-1)^k}{2^{m+1-k}} (p_{1,m,k-1} + 4(k+1)p_{1,m,k}) w^k \vec{z} \\
& + \sum_{k=0}^{m-1} \frac{(-1)^k}{2^{m-k}} (p_{1,m,k} + 4(k+1)p_{1,m,k+1}) w^k \vec{e} + (-1)^m p_{1,m,m} w^m \vec{e}
\end{aligned} \tag{B.57}$$

(B.28) and (B.27) give us the following identities.

$$\begin{aligned}
p_{1,m,k} + 4(k+1)p_{1,m,k+1} &= p_{2,m,k} \\
p_{1,m,k-1} + 4(k+1)p_{1,m,k} &= p_{2,m,k-1} + 4p_{1,m,k} \\
p_{1,m,m} &= p_{2,m,m}
\end{aligned}$$

Applying the above identities to (B.57), we have

$$\begin{aligned}
& g^{-(m+1)} \exp(ar^2) \nabla^{2m+2} \times B \\
& = \frac{2}{2^m} p_{1,m,0} \vec{z} + (-1)^{m+1} p_{1,m,m} w^{m+1} \vec{z} \\
& + \sum_{k=1}^m \frac{(-1)^k}{2^{m+1-k}} (p_{2,m,k-1} + 4p_{1,m,k}) w^k \vec{z} \\
& + \sum_{k=0}^{m-1} \frac{(-1)^k}{2^{m-k}} p_{2,m,k} w^k \vec{e} + (-1)^m p_{2,m,m} w^m \vec{e}
\end{aligned}$$

The above equation can be rearranged into

$$\begin{aligned}
& g^{-(m+1)} \exp(ar^2) \nabla^{2m+2} \times B \\
&= \sum_{k=0}^{m+1} \frac{(-1)^k}{2^{m+1-k}} (p_{2,m,k-1} + 4p_{1,m,k}) w^k \vec{z} \\
&+ \sum_{k=0}^m \frac{(-1)^k}{2^{m-k}} p_{2,m,k} w^k \vec{e}
\end{aligned}$$

By (B.34), we have

$$\begin{aligned}
g^{-(m+1)} \exp(ar^2) \nabla^{2m+2} \times B &= \sum_{k=0}^m \frac{(-1)^k}{2^{m-k}} p_{2,m,k} w^k \vec{e} \\
&+ \sum_{k=0}^m \frac{(-1)^k}{2^{m-k}} (2p_{1,m,k} - wp_{2,m,k}) w^k \vec{z}
\end{aligned}$$

The above equation shows that (B.56) holds for  $n = m$ .

Applying the curl operation on both side of (B.56) with  $n = m$  and using (B.52), we have

$$\begin{aligned}
\nabla^{2(m+1)+1} \times B &= g^{m+1} \exp(-ar^2) (\nabla - g\vec{s}) \times \\
&\left( \sum_{k=0}^m \frac{(-1)^k}{2^{m-k}} (2p_{1,m,k} - wp_{2,m,k}) w^k \vec{z} + \sum_{k=0}^m \frac{(-1)^k}{2^{m-k}} p_{2,m,k} w^k \vec{e} \right)
\end{aligned}$$

Moving the factor  $g^{m+1} \exp(-ar^2)$  to the left hand side for cleanness, the above equation can be written as

$$\begin{aligned}
& g^{-(m+1)} \exp(ar^2) \nabla^{2(m+1)+1} \times B \\
&= \sum_{k=0}^m \frac{(-1)^k}{2^{m-k}} (3p_{1,m,k} \nabla \times w^k \vec{z} - p_{2,m,k} \nabla \times w^{k+1} \vec{z}) \\
&+ \sum_{k=0}^m \frac{(-1)^k}{2^{m-k}} p_{2,m,k} \nabla \times w^k \vec{e} \\
&- \sum_{k=0}^m \frac{(-1)^k}{2^{m-k}} (2p_{1,m,k} - wp_{2,m,k}) w^k g\vec{s} \times \vec{z} \\
&- \sum_{k=0}^m \frac{(-1)^k}{2^{m-k}} p_{2,m,k} w^k g\vec{s} \times \vec{e}
\end{aligned}$$

Applying (B.47), (B.48), (B.49), (B.50) and (B.51), we have

$$\begin{aligned}
& g^{-(m+1)} \exp(ar^2) \nabla^{2(m+1)+1} \times B \\
&= \sum_{k=1}^m \frac{k=0}{2^{m-k}} 4k p_{1,m,k} w^{k-1} \vec{h} \\
&\quad - \sum_{k=0}^m \frac{(-1)^k}{2^{m-k}} p_{2,m,k} 2(k+1) w^k \vec{h} \\
&\quad - \sum_{k=0}^m \frac{(-1)^k}{2^{m-k}} p_{2,m,k} w^k \vec{h} \\
&\quad - \sum_{k=0}^m \frac{(-1)^k}{2^{m-k}} (2p_{1,m,k} - w p_{2,m,k}) w^k \vec{h}
\end{aligned}$$

By (B.34), the above can be written as

$$\begin{aligned}
& g^{-(m+1)} \exp(ar^2) \nabla^{2(m+1)+1} \times B \\
&= \sum_{k=1}^m \frac{(-1)^k}{2^{m-k}} 4k p_{1,m,k} w^{k-1} \vec{h} \\
&\quad - \sum_{k=0}^m \frac{(-1)^k}{2^{m-k}} p_{2,m,k} 2(k+1) w^k \vec{h} \\
&\quad - \sum_{k=0}^m \frac{(-1)^k}{2^{m-k}} p_{2,m,k} w^k \vec{h} \\
&\quad - \sum_{k=0}^{m+1} \frac{(-1)^k}{2^{m+1-k}} (p_{2,m,k-1} + 4p_{1,m,k}) w^k \vec{h}
\end{aligned}$$

Rearrange the summations into

$$g^{-(m+1)} \exp(ar^2) \nabla^{2(m+1)+1} \times B = \sum_{k=0}^m \frac{(-1)^{k+1}}{2^{m+1-k}} v_{m,k} w^k \vec{h} + (-1)^m w^{m+1} \vec{h} \quad (\text{B.58})$$

where

$$v_{m,k} = p_{2,m,k} 2(2k+3) + p_{2,m,k-1} + 4(4(k+1)p_{1,m,k+1} + p_{1,m,k})$$

By (B.28), we have

$$v_{m,k} = 2(2k+5)p_{2,m,k} + p_{2,m,k-1}$$

By (B.30),

$$v_{m,k} = p_{1,m+1,k}$$

Thus, (B.58) becomes

$$g^{-(m+1)} \exp(ar^2) \nabla^{2(m+1)+1} \times B = \sum_{k=0}^m \frac{(-1)^{k+1}}{2^{m+1-k}} p_{1,m+1,k} w^k \vec{h} + (-1)^m w^{m+1} \vec{h}$$

The above can be written as

$$g^{-(m+1)} \exp(ar^2) \nabla^{2(m+1)+1} \times B = \sum_{k=0}^{m+1} \frac{(-1)^{k+1}}{2^{m+1-k}} p_{1,m+1,k} w^k \vec{h}$$

The above shows that (B.55) holds for  $n = m + 1$ .

$\therefore$  By the principle of induction, (B.55) and (B.56) hold for all  $n \in \mathbb{Z}_{\geq 0}$ .  $\square$

## References

- [1] K. Yee, Numerical solution of initial boundary value problems involving Maxwell's equations in isotropic media, *IEEE Transactions on Antennas and Propagation* 14 (3) (1966) 302–307. doi:10.1109/TAP.1966.1138693.
- [2] A. Oskooi, D. Roundy, M. Ibanescu, P. Bermel, J. Joannopoulos, S. Johnson, MEEP: A flexible free-software package for electromagnetic simulations by the FDTD method, *Computer Physics Communications* 181 (2010) 687–702.
- [3] J. Schneider, *Understanding the Finite-Difference Time-Domain Method* (2025).  
URL <https://eecs.wsu.edu/~schneidj/ufdtd/ufdtd.pdf>
- [4] J. von Neumann, R. Richtmyer, A method for the numerical calculation of hydrodynamic shocks, *Journal of Applied Physics* 21 (3) (1950) 232–237. doi:10.1063/1.1699639.
- [5] L. Zhou, Z. Mu, Y. Pu, X. Xi, Long-range Loran-C ground-wave propagation prediction based on adaptive moving window finite-difference time-domain method with compute unified device architecture parallel computing techniques, *IET Microwaves, Antennas and Propagation* (Oct. 2014). doi:10.1049/iet-map.2014.0312.
- [6] A. Fedeli, C. Montecucco, G. L. Gragnani, Open-Source Software for Electromagnetic Scattering Simulation: The Case of Antenna Design, *Electronics* 8 (1506) (Oct. 2019). doi:10.3390/electronics8121506.
- [7] A. F. Mastryukov, A Finite-Difference Scheme for the One-Dimensional Maxwell Equations, *Numer. Analys. Appl.* 13 (2020) 57–67. doi:10.1134/S199542392001005X.

- [8] J. B. Schneider, C. L. Wagner, FDTD Dispersion Revisited: Faster-Than-Light Propagation, *IEEE MICROWAVE AND GUIDED WAVE LETTERS* 9 (2) (1999) 54–56.
- [9] H. Kohlmann, FDTD Simulation of Lightning Electromagnetic Fields An approach with the software package MEEP, MASTER THESIS, TECHNISCHE UNIVERSITÄT WIEN Vienna Austria (2020).
- [10] C. W. Manry, S. L. Broschat, J. B. Schneider, Higher-Order FDTD Methods for Large Problems, *J. Applied Computational Electromagnetics Society* 10 (2) (1995).
- [11] O. D. Jefimenko, Solutions of Maxwell’s equations for electric and magnetic fields in arbitrary media, *American Journal of Physics* 60 (10) (1992) 899–902.
- [12] O.-Z. Lipan, A. D. Sabata, Optimizing bi-layered periodic structures: a closed-form transfer matrix method based on pendry-mackinnon’s discrete maxwell’s equations, *J. Opt. Soc. Am. B* 41 (2) (2024) A116–A125. doi:10.1364/JOSAB.497185.
- [13] E. L. Boudec, C. Kasmi, N. Mora, F. Rachidi, E. Radici, M. Rubinstein, F. Vega, The time-domain cartesian multipole expansion of electromagnetic fields, *Scientific Reports* 14 (1) (2024). doi:10.1038/s41598-024-58570-1. URL <https://doi.org/10.1038/s41598-024-58570-1>
- [14] H. Yang, X. Zeng, X. Wu, An approach to solving maxwell’s equations in time domain, *Journal of Mathematical Analysis and Applications* 518 (1) (2023) 126678. doi:<https://doi.org/10.1016/j.jmaa.2022.126678>.
- [15] D. W. Ge, Analytical solutions of 1D Maxwell’s equations via infinite-order expansions, *Results in Applied Mathematics* 29 (2026) 100688. doi:<https://doi.org/10.1016/j.rinam.2026.100688>.